

TBG II: Stable Symmetry Anomaly in Twisted Bilayer Graphene

Zhi-Da Song,¹ Biao Lian,¹ Nicolas Regnault,^{1,2} and B. Andrei Bernevig¹,

¹*Department of Physics, Princeton University, Princeton, New Jersey 08544, USA*

²*Laboratoire de Physique de l'Ecole normale supérieure,*

ENS, Université PSL, CNRS, Sorbonne Université,

Université Paris-Diderot, Sorbonne Paris Cité, Paris, France

(Dated: October 28, 2020)

We show that the entire continuous model of twisted bilayer graphene (TBG) (and not just the two active bands) with particle-hole symmetry is anomalous and hence incompatible with lattice models. Previous works, *e.g.*, [Phys. Rev. Lett. 123, 036401], [Phys. Rev. X 9, 021013], [Phys. Rev. B 99, 195455], and others [1–4] found that the two flat bands in TBG possess a fragile topology protected by the $C_{2z}T$ symmetry. [Phys. Rev. Lett. 123, 036401] also pointed out an approximate particle-hole symmetry (\mathcal{P}) in the continuous model of TBG. In this work, we numerically confirm that \mathcal{P} is indeed a good approximation for TBG and show that the fragile topology of the two flat bands is enhanced to a \mathcal{P} -protected stable topology. This stable topology implies $4l+2$ ($l \in \mathbb{N}$) Dirac points between the middle two bands. The \mathcal{P} -protected stable topology is robust against arbitrary gap closings between the middle two bands and the other bands. We further show that, remarkably, this \mathcal{P} -protected stable topology, as well as the corresponding $4l+2$ Dirac points, cannot be realized in lattice models that preserve both $C_{2z}T$ and \mathcal{P} symmetries. In other words, the continuous model of TBG is anomalous and cannot be realized on lattices. Two other topology related topics, with consequences for the interacting TBG problem, *i.e.*, the choice of Chern band basis in the two flat bands and the perfect metal phase of TBG in the so-called second chiral limit, are also discussed.

I. Introduction

TBG at the first magic angle ($\theta \approx 1.05^\circ$) exhibits a group of two almost exactly flat bands [5]. Due to the interesting interaction insulating and conducting states [6–36], superconductor states [37–55], and single-particle topology [1–3, 23, 56–66] in the flat bands, TBG represents one of the most versatile physical systems of recent years [1–21, 23–35, 37–64, 66–113]. Refs. [56, 58] showed that the $C_{2z}T$ symmetry of TBG protects a fragile topology [80, 114–118] of the two flat bands, which is characterized by a \mathbb{Z} -valued winding number. The fragile topology manifests itself as a topological obstruction for exponentially decaying Wannier functions satisfying $C_{2z}T$ symmetry for the two flat bands. However, the Wannier obstruction can be removed by adding trivial bands into the consideration [80, 114, 115]. For example, Ref. [57] showed explicitly that symmetric Wannier functions can be constructed if certain additional orbitals are coupled to the fragile topological band protected by $C_{2z}T$. However, the papers arguing for a trivialization of the bands [56, 57] neglected one (approximate) symmetry of the TBG model [5].

The Bistritzer MacDonald (BM) model [5] of TBG has an approximate particle-hole symmetry \mathcal{P} first pointed out in Ref. [58]. It was already pointed out in Ref. [58] that with this approximate symmetry, there seems to be a further, stable topology in TBG, but this result was not further expanded. We here numerically confirm that the error - on the wavefunctions - of the \mathcal{P} symmetry

(defined in Section II B) in the BM model of TBG is extremely small (< 0.01). Thus we count \mathcal{P} symmetry as a good approximation for the low energy physics in TBG. We prove that if the $C_{2z}T$ protected winding number of the two flat bands is odd (true in TBG), then the two flat bands have a stable topology protected by \mathcal{P} , which is characterized by a \mathbb{Z}_2 invariant δ . In contrast to the fragile topological bands, which can be trivialized by being coupled to certain trivial bands, the \mathbb{Z}_2 topology, as well as the Wannier obstruction implied by the \mathbb{Z}_2 invariant, is stable against adding trivial bands that preserve the \mathcal{P} symmetry. We further proved that, in the presence of $C_{2z}T$ and \mathcal{P} , the \mathbb{Z}_2 invariant δ of $2M$ particle-hole symmetric bands $\epsilon_{-M}(\mathbf{k}) \cdots \epsilon_{-1}(\mathbf{k}), \epsilon_1(\mathbf{k}) \cdots \epsilon_M(\mathbf{k})$ is related to the number of Dirac points N_D between $\epsilon_{-1}(\mathbf{k})$ and $\epsilon_1(\mathbf{k})$ in the first Brillouin zone (BZ) as $\delta = \frac{N_D}{2} \bmod 2$, provided that the $2M$ bands are gapped from higher and lower bands. Here $\epsilon_n(\mathbf{k})$ ($\epsilon_{-n}(\mathbf{k})$) is the n -th positive (negative) band. Therefore, as long as $4l+2$ ($l \in \mathbb{N}$) Dirac points exist between $\epsilon_{-1}(\mathbf{k})$ and $\epsilon_1(\mathbf{k})$ we find that $2M, \forall M \in \mathbb{N}$ particle-hole symmetric bands (separate in energy from the $M+1, M+2, \dots$ and $\dots, -M-2, -M-1$ bands) have $\delta = 1$ and hence are topologically nontrivial. The feature of TBG that arbitrary $2M$ bands are topological is inconsistent with lattice models with $C_{2z}T$ and \mathcal{P} symmetry. In a lattice model, if $2M$ is large enough, *e.g.*, equals to the number of orbitals in the model, the $2M$ bands have to be topologically trivial because they span the Hilbert space of the local orbitals. Therefore, the \mathbb{Z}_2 topology, and the $4l+2$ Dirac points accordingly, cannot be realized in lattice models with finite number of orbitals. We hence call the \mathbb{Z}_2 topology an anomaly of the $C_{2z}T$ and \mathcal{P} symmetries. We further note that this implies that the many-body $U(4)$ and $U(4) \times U(4)$ symme-

* bernevig@princeton.edu

tries [110–112] are incompatible with a lattice model and hence anomalous. It also implies that the lattice models build to model TBG [1, 2, 23, 57] have to break the \mathcal{P} symmetry or the $C_{2z}T$ symmetry of the TBG model.

This paper is organized as follows. In Section II, we present a review of the BM model of TBG and summarize its symmetries. The error of the approximate particle-hole symmetry \mathcal{P} is defined and is confirmed as being small (< 0.01). In Section III, we prove that the \mathcal{P} symmetry protects a stable \mathbb{Z}_2 topological state. In Section IV, a no-go theorem of the \mathbb{Z}_2 topology is proved for lattice models with the $C_{2z}T$ and \mathcal{P} symmetries. The relation between the \mathbb{Z}_2 invariant and the number of Dirac points is also established in this section. In Section V, we show that, when the two flat bands are gapped from the other bands, there is natural choice of Chern band basis (with opposite Chern numbers) in the two flat bands. The Chern band basis is used in our interacting works [110–113] on TBG. In Section VI, we show that, in the so-called second chiral limit, defined in [110] as the second limit having an interacting extended $U(4) \times U(4)$ symmetry, the symmetry anomaly of TBG manifests as a perfect metal phase, where all the bands are connected to each other. A brief summary of this work is given in Section VII.

II. The BM model of twisted bilayer graphene and its symmetries

We first present a short review of the BM model. A more detailed account can be found in supplementary material of Ref. [58].

A. A brief review of the BM model

TBG is an engineered material of two graphene layers twisted by a small angle θ from each other. The band structure of each of the two layers exhibits two Dirac points at the K and K^0 momenta in the single layer Brillouin zone (BZ), respectively; the two Dirac points are related by time-reversal T . Thus the band structure of TBG exhibits four Dirac points: two from the top layer and the other two from the bottom layer. When θ is small such that the interlayer coupling is smooth in real space - with a length scale much larger than the atom distances - the graphene valley (K and K^0) is a good quantum number of low energy states of TBG [5]. In this case, the states around K (K^0) in the top layer only couple to the states around K (K^0) in the bottom layer. Therefore, the low energy band structure of TBG decomposes into two independent graphene valleys, and each valley has two Dirac points originated from the two layers, respectively. In this work, we will focus on the valley K . The bands in the other valley K^0 can be obtained by acting T on the bands in the valley K .

We assume the top single graphene layer is rotated

from the x -direction by an angle $\frac{\theta}{2}$ (rotation axis is z). Thus the Dirac Hamiltonian around K in the top layer is $-iv_F\partial_x(\cos\frac{\theta}{2}\sigma_x - \sin\frac{\theta}{2}\sigma_y) - iv_F\partial_y(\cos\frac{\theta}{2}\sigma_y + \sin\frac{\theta}{2}\sigma_x) \approx -iv_F\partial_{\mathbf{r}} \cdot \boldsymbol{\sigma} + i\frac{\theta}{2}v_F\partial_{\mathbf{r}} \times \boldsymbol{\sigma}$, where v_F is the Fermi-velocity of single-layer graphene and $\boldsymbol{\sigma} = (\sigma_x, \sigma_y)$ are Pauli matrices representing the A/B sublattices of graphene. The bottom layer is rotated from the x -direction by an angle $-\frac{\theta}{2}$. Correspondingly, the Dirac Hamiltonian around K in the bottom layer is $-iv_F\partial_{\mathbf{r}} \cdot \boldsymbol{\sigma} - i\theta v_F\partial_{\mathbf{r}} \times \boldsymbol{\sigma}$. The interlayer coupling is encoded in a position dependent matrix $T(\mathbf{r})$, where $\mathbf{r} = (x, y)$, such that the Hamiltonian of TBG, to linear order of θ , can be written as

$$H(\mathbf{r}) = -iv_F \left(\tau_0 \partial_{\mathbf{r}} \cdot \boldsymbol{\sigma} - \frac{\theta}{2} \tau_z \partial_{\mathbf{r}} \times \boldsymbol{\sigma} \right) + \begin{pmatrix} 0 & T(\mathbf{r}) \\ T^\dagger(\mathbf{r}) & 0 \end{pmatrix}. \quad (1)$$

Here τ_0 and τ_z are the two-by-two identity matrix and the third Pauli matrix for the layer degree of freedom, respectively. According to Ref. [5], when θ is small ($\sim 1^\circ$), $T(\mathbf{r})$ forms a smooth moiré potential:

$$T(\mathbf{r}) = \sum_{i=1}^3 e^{i\mathbf{q}_i \cdot \mathbf{r}} T_i, \quad (2)$$

where \mathbf{q}_i 's are $\mathbf{q}_1 = k_D(0, -1)$, $\mathbf{q}_2 = k_D(\frac{p}{2}, \frac{1}{2})$, $\mathbf{q}_3 = k_D(-\frac{p}{2}, \frac{1}{2})$, with $k_D = 2|K|\sin\frac{\theta}{2}$ being the distance between K momenta in the two layers, and T_i 's are

$$T_i = w_0 \sigma_0 + w_1 \left[\sigma_x \cos \frac{2\pi(i-1)}{3} + \sigma_y \sin \frac{2\pi(i-1)}{3} \right], \quad (3)$$

where w_0 and w_1 are two constant parameters. Since the w_0 term contributes to the diagonal elements, it represents the interlayer coupling between the A(B) sublattice of the top layer and the A(B) sublattice of the bottom layer. Similarly, the w_1 term only contributes to the off-diagonal elements, it is thus associated to the interlayer coupling between A(B) sublattice of the top layer and B(A) sublattice of the bottom layer.

The moiré potential (Eq. (2)) is invariant (up to a gauge transformation) under the translations $\mathbf{a}_{M1} = \frac{2\pi}{k_D}(\frac{p}{3}, \frac{1}{3})$, $\mathbf{a}_{M2} = \frac{2\pi}{k_D}(-\frac{p}{3}, \frac{1}{3})$. The translation symmetry of the moiré potential is manifest in real space (Fig. 1a). The corresponding reciprocal lattice bases are $\mathbf{b}_{M1} = \mathbf{q}_2 - \mathbf{q}_1$, $\mathbf{b}_{M2} = \mathbf{q}_3 - \mathbf{q}_1$ (Fig. 1b). The unit cell spanned by \mathbf{a}_{M1} and \mathbf{a}_{M2} is referred to as the moiré unit cell. Each moiré unit cell has one AA region, one AB region, and one BA region. In the AA region, the A(B) sublattice of the top layer sit on top of the A(B) sublattice of the bottom layer; in the AB region, the A and B sublattices of the top layer sit on top of the B sublattices and the empty hexagon centers of the bottom layer, respectively; in the BA region, the B and A sublattices of the upper layer sit on top of the A sublattices and the empty hexagon centers of the lower layer, respectively. First principle calculations show that the two layers are corrugated in the z -direction [119–122]. The distance between the two layers in the AA region is larger than the

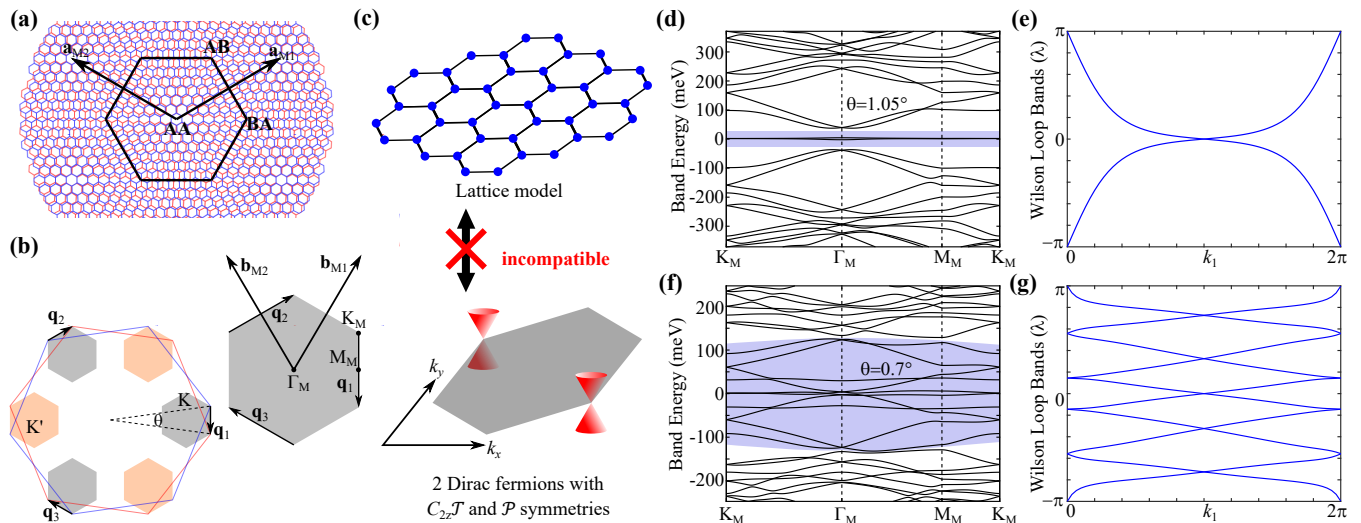


FIG. 1. The lattice, symmetry anomaly, band structures, and Wilson loop bands of TBG. **(a)** The moiré unit cell, where the blue sheet and the red sheet represent the top and bottom layers, respectively. In the AA, AB, BA regions, the A sublattice of the top layer are located above the A sublattice, the B sublattice, and the hexagon center of the bottom layer, respectively. **(b)** The moiré Brillouin zone. Left: The grey and yellow hexagons represent the moiré Brillouin zone for the graphene valleys K and K' , respectively. Right: The reciprocal lattices and the high symmetry momenta of the moiré Brillouin zone in graphene valley K . **(c)** $4l + 2$ ($l \in \mathbb{N}$) Dirac points cannot be realized in lattice models with $C_{2z}T$ and \mathcal{P} symmetries. **(d-e)** The band structure and Wilson loop bands of the middle two bands (shaded) at $\theta = 1.05^\circ$. The crossings in Wilson loop bands are protected by $C_{2z}T$ and/or the approximate \mathcal{P} . Each Wilson loop operator is integrated along \mathbf{b}_{M2} and the spectrum is plotted along \mathbf{b}_{M1} . **(f-g)** The band structure and Wilson loop bands of the middle ten bands (shaded) at $\theta = 0.7^\circ$. The crossings at $\lambda = 0, \pi$ in the Wilson loop bands are protected by $C_{2z}T$ and/or by the approximate \mathcal{P} ; the double degeneracies with $\lambda \neq 0, \pi$ at $k_1 = 0, \pi$ are protected by the approximate \mathcal{P} . These double-degeneracies guarantee Wilson loop flow for any bands with $4n + 2$ Dirac nodes at zero energy. In fact, we have kept the \mathcal{P} -breaking term $i\theta v_F \tau_z \partial_{\mathbf{r}} \times \boldsymbol{\sigma}$ (Eq. (1)) in the calculations used to generate this plot, which would split the double degeneracies in principle. However, the splittings are almost invisible by eye in the plot, implying that the \mathcal{P} symmetry is a good approximation. The degeneracies are exact when P is exact. The parameters of Hamiltonian used in (d-g) are $v_F = 5.944\text{eV} \cdot \text{\AA}$, $|K| = 1.703\text{\AA}^{-1}$, $w_1 = 110\text{meV}$, $w_0 = 0.7w_1$.

distance in the AB and BA regions. Since w_0 and w_1 are mainly dominated by the couplings in the AA and AB/BA regions [5], respectively, this implies that, in the realistic model, w_0 is smaller than w_1 [2]. In Figs. 1d and 1f, we show the band structures for two different twist angles $\theta = 1.05, 0.7^\circ$. The parameters are set as $v_F = 5.944\text{eV} \cdot \text{\AA}$, $|K| = 1.703\text{\AA}^{-1}$, $w_1 = 110\text{meV}$, $w_0 = 0.7w_1$.

B. Symmetries of the BM model

The model Eq. (1) has several point group symmetries: (i) $C_{2z}T = \sigma_x K$, where K is the complex conjugation, (ii) $C_{3z} = e^{i\frac{2\pi}{3}\sigma_z}$, (iii) $C_{2x} = \tau_x \sigma_x$. One can verify that the Hamiltonian is invariant under these symmetries. Notice that the single-graphene-valley Hamiltonian does not have the C_{2z} rotation and the time-reversal T symmetries since they map one graphene valley to the other. The three crystalline symmetries and the moiré translations generate the magnetic space group $P6^0_2O_2$ (#177.151 in the BNS setting [123]) [58].

We define a unitary particle-hole operation $P = i\tau_y$, which transforms the position as $\mathbf{r} \rightarrow -\mathbf{r}$ [58]. Here $\tau_{x,y,z}$

are Pauli matrices representing the layer degree of freedom. Under P the Hamiltonian transforms as

$$PH(\mathbf{r})P^\dagger = -H(-\mathbf{r}) + i\theta v_F \tau_z \partial_{\mathbf{r}} \times \boldsymbol{\sigma}. \quad (4)$$

When $\theta \sim 1$, the second term on the right hand side is of order $0.018v_F k_D$ and hence is much smaller than the energy scale of the low energy physics, which is of order $v_F k_D$. Therefore, P is an emergent anticommuting symmetry when θ is small. It satisfies the algebra [58]:

$$[C_{2z}T, P] = [C_{3z}, P] = 0, \{C_{2x}, P\} = 0, P^2 = -1. \quad (5)$$

For later convenience, we define an anti-unitary particle operation $\mathcal{P} = PC_{2z}T = i\tau_y \sigma_x K$, which is local in real space and satisfies $\mathcal{P}^2 = -1$. It acts on the Hamiltonian as

$$\mathcal{P}H(\mathbf{r})\mathcal{P}^{-1} = -H(\mathbf{r}) + i\theta v_F \tau_z \partial_{\mathbf{r}} \times \boldsymbol{\sigma}. \quad (6)$$

We can also define a chiral operation $C = \sigma_z$, which is local in real space. [59]. Under C the Hamiltonian transforms as

$$CH(\mathbf{r})C^\dagger = -H(\mathbf{r}) + 2w_0 \tau_x \sigma_0 \sum_{i=1}^3 e^{i\mathbf{q}_i \cdot \mathbf{r}}. \quad (7)$$

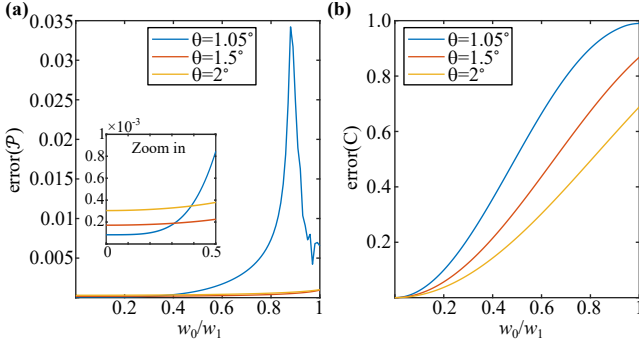


FIG. 2. Errors of the approximate symmetries \mathcal{P} (a) and C (b) on the wavefunctions (as defined in Eqs. 9 and 10) in TBG as functions of w_0/w_1 . Here we change w_0 while keeping w_1 fixed (110meV). The errors are shown for different values of the twist angle $\theta = 1.05^\circ, 1.5^\circ, 2^\circ$.

In the so-called chiral limit [59], *i.e.*, $w_0 = 0$, the second term on the right hand of side vanishes and hence C become an emergent anticommuting symmetry. The chiral symmetry satisfies the algebra

$$\{C_{2z}T, C\} = \{C_{2x}, C\} = 0, [C_{3z}, C] = [P, C] = 0, C^2 = 1. \quad (8)$$

We numerically checked how much \mathcal{P} and C are broken in the *wavefunctions* of the model Eq. (1). To be specific, we define the errors of the two symmetries in the two flat bands as

$$\text{error}(\mathcal{P}) = 1 - \int \frac{d^2\mathbf{k}}{(2\pi)^2} |\langle u_{1,\mathbf{k}} | \mathcal{P} | u_{1,\mathbf{k}} \rangle|^2, \quad (9)$$

$$\text{error}(C) = 1 - \int \frac{d^2\mathbf{k}}{(2\pi)^2} |\langle u_{1,\mathbf{k}} | C | u_{1,\mathbf{k}} \rangle|^2, \quad (10)$$

respectively, where $|u_{1,\mathbf{k}}\rangle$ and $|u_{1,\mathbf{k}}\rangle$ are the periodic parts of the Bloch states of the highest occupied band and the lowest empty band at charge neutrality, respectively. When the two symmetries are exact, we have $|\langle u_{1,\mathbf{k}} | \mathcal{P} | u_{1,\mathbf{k}} \rangle| = |\langle u_{1,\mathbf{k}} | S | u_{1,\mathbf{k}} \rangle| = 1$ and hence the errors are zero. Using the parameters $v_F = 5.933\text{eV} \cdot \text{\AA}$, $|K| = 1.703\text{\AA}^{-1}$, $w_1 = 110\text{meV}$, we plot $\text{error}(\mathcal{P})$ and $\text{error}(C)$ as functions of w_0/w_1 (with fixed w_1) for a few twist angles in Fig. 2. For $\theta = 1.05^\circ$, $\text{error}(\mathcal{P})$ is small (< 0.01) for $w_0 \leq 0.82w_1$, thus the \mathcal{P} symmetry is a good approximation for TBG, while the C symmetry only starts being good (with $\text{error} < 0.01$) for $w_0 \leq 0.07w_1$.

III. Stable topology protected by particle-hole symmetry \mathcal{P}

A. The Wilson loop \mathbb{Z}_2 invariant protected by \mathcal{P}

We denote the Hamiltonian in momentum space as $H(\mathbf{k})$. We assume the emergent anti-unitary particle-hole

symmetry, *i.e.*, $\mathcal{P}H(\mathbf{k})\mathcal{P}^{-1} = -H(-\mathbf{k})$, and $\mathcal{P}^2 = -1$. As detailed in Section II B, $\mathcal{P} = PC_{2z}T$ is anti-unitary and squares to -1, and is the product of the unitary P of Ref. [58] and $C_{2z}T$. We denote the energy and the periodic part of Bloch state of the n -th band above (below) the zero energy as $\epsilon_n(\mathbf{k})$ ($\epsilon_{-n}(\mathbf{k})$) and $|u_n(\mathbf{k})\rangle$ ($|u_{-n}(\mathbf{k})\rangle$), respectively. As explained in Appendix A and in Ref. [58], $|u_n(\mathbf{k})\rangle$ satisfies the periodicity $|u_n(\mathbf{k} + \mathbf{G})\rangle = V^{\mathbf{G}}|u_n(\mathbf{k})\rangle$, with \mathbf{G} being a reciprocal lattice and $V^{\mathbf{G}}$ a unitary matrix referred to as the embedding matrix. Since \mathcal{P} anti-commutes with the Hamiltonian and flips the momentum, we have $\epsilon_n(\mathbf{k}) = -\epsilon_{-n}(-\mathbf{k})$. The state $\mathcal{P}|u_n(\mathbf{k})\rangle$ must have the momentum $-\mathbf{k}$ and the energy $\epsilon_{-n}(-\mathbf{k})$. In general, $\mathcal{P}|u_n(\mathbf{k})\rangle$ is spanned by Bloch states at $-\mathbf{k}$ as

$$\mathcal{P}|u_n(\mathbf{k})\rangle = \sum_{n'} |u_{n'}(-\mathbf{k})\rangle B_{n'n}^{(\mathcal{P})}(\mathbf{k}), \quad (11)$$

where the summation over n' is limited to those satisfying $\epsilon_{n'}(\mathbf{k}) = -\epsilon_n(-\mathbf{k})$, and $B_{n'n}^{(\mathcal{P})}(\mathbf{k})$ is a unitary matrix referred to as the sewing matrix of \mathcal{P} . $B^{(\mathcal{P})}(\mathbf{k})$ is periodic in momentum space, *i.e.*, $B^{(\mathcal{P})}(\mathbf{k} + \mathbf{G}) = B^{(\mathcal{P})}(\mathbf{k})$ [124, 125]. Since $\mathcal{P}^2 = -1$, it should satisfy

$$B^{(\mathcal{P})}(-\mathbf{k})B^{(\mathcal{P})}(\mathbf{k}) = -1. \quad (12)$$

Multiplying $B^{(\mathcal{P})T}(\mathbf{k})$ on the right hand side of the above equation, we obtain

$$B^{(\mathcal{P})}(-\mathbf{k}) = -B^{(\mathcal{P})T}(\mathbf{k}). \quad (13)$$

We now prove that the \mathcal{P} symmetry protects a \mathbb{Z}_2 invariant for $2M$ particle-hole symmetric separate bands, *i.e.*, bands $\epsilon_M(\mathbf{k}), \epsilon_{M+1}(\mathbf{k}) \cdots \epsilon_M(\mathbf{k})$, gapped from higher and lower bands. This proof is not limited to TBG but applies to any system having our anti-unitary \mathcal{P} symmetry. We introduce the matrix $U(\mathbf{k}) = (|u_M(\mathbf{k})\rangle, |u_{M+1}(\mathbf{k})\rangle \cdots |u_M(\mathbf{k})\rangle)$. We parameterize \mathbf{k} as $k_1\mathbf{b}_1 + k_2\mathbf{b}_2$, where \mathbf{b}_1 and \mathbf{b}_2 are the reciprocal lattice basis vectors. Then we define the Wilson loop operator of the $2M$ bands for a given k_1 as

$$W(k_1) = \lim_{N \rightarrow \infty} \prod_{j=0}^{N-1} U^y(k_1, j \frac{2\pi}{N}) U(k_1, (j+1) \frac{2\pi}{N}). \quad (14)$$

The order of the matrices in the product is given by j : matrices with larger k_2 ($= j \frac{2\pi}{N}$) always appear on the right hand side of matrices with smaller k_2 . Due to the periodicity of Bloch states, $W(k_1)$ is periodic. Since $W(k_1)$ is unitary, its eigenvalues are phase factors $e^{i\lambda_n(k_1)}$ ($n = 1 \cdots 2M$), where $\lambda_n(k_1)$ ranges from $-\pi$ to π . $\{\lambda_n(k_1)\}$ are called as the Wilson loop bands. Topology is usually a result of Wilson loop flow, which in turn is a result of unavoidable crossings between Wilson loop bands.

We now prove that the Wilson loop bands are doubly degenerate at $k_1 = 0$ and $k_1 = \pi$, as shown in Fig. 3a-c. In fact, we should heuristically expect this, since the

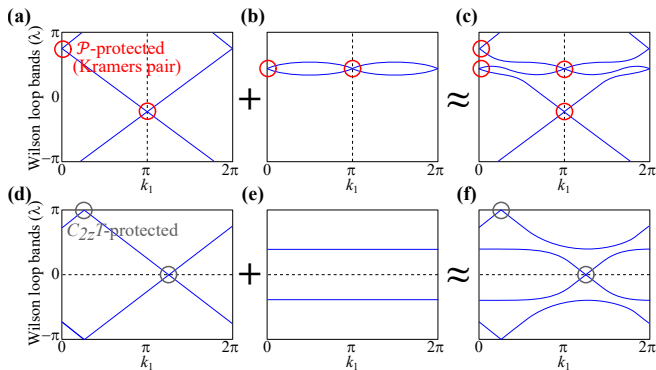


FIG. 3. Comparison of Wilson loop windings protected by \mathcal{P} and $C_{2z}T$. (a-c) The Wilson loop bands with \mathcal{P} . The crossings at $k_1 = 0, \pi$ are Kramers pairs protected by \mathcal{P} . The \mathbb{Z}_2 invariant (a) equals to 1 if the Wilson loop bands form a zigzag connection between $k_1 = 0$ and $k_1 = \pi$ and (b) equals to 0 otherwise. The \mathcal{P} -protected topology is stable against adding trivial bands: Coupling the nontrivial Wilson loop bands (a) to a trivial Wilson loop bands (b) yields a nontrivial Wilson loop bands (c). (d-f) The Wilson loop bands with $C_{2z}T$. The crossings at $\lambda = 0, \pi$ are protected by $C_{2z}T$. For a two-band system, the topology is nontrivial if the Wilson loop bands winds (d) and is trivial otherwise (e). The $C_{2z}T$ -protected topology is fragile: Coupling the nontrivial Wilson loop bands (d) to a trivial Wilson loop bands (f) yields a trivial Wilson loop bands (f).

Wilson loop respects \mathcal{P} as it contains all bands related by the particle-hole symmetry. Since \mathcal{P} is anti-unitary and squares to -1 is hence acts as spinful time-reversal, which we already know to enforce Kramers doublets in the Wilson loop spectrum [126, 127]. Due to Eq. (11), we have

$$\begin{aligned} \langle u_n(\mathbf{k}) | u_{n'}(\mathbf{k}^0) \rangle &= \langle \mathcal{P} u_{n'}(\mathbf{k}^0) | \mathcal{P} u_n(\mathbf{k}) \rangle \\ &= \sum_{mm'} B_{m'n'}^{(\mathcal{P})}(\mathbf{k}^0) \langle u_{m'}(-\mathbf{k}^0) | u_m(-\mathbf{k}) \rangle B_{mn}^{(\mathcal{P})}(\mathbf{k}). \end{aligned} \quad (15)$$

In the above equation we have made use of a property of anti-unitary symmetries: for any two states $|\phi\rangle, |\psi\rangle$ and an arbitrary anti-unitary operator \mathcal{O} , we have $\langle \phi | \psi \rangle = \langle \mathcal{O}\psi | \mathcal{O}\phi \rangle$. Substituting this relation into Eq. (14) and using the periodicity relations $B^{(\mathcal{P})}(\mathbf{k} + \mathbf{G}) = B^{(\mathcal{P})}(\mathbf{k})$ and $|u_n(\mathbf{k} + \mathbf{G})\rangle = V^{\mathbf{G}}|u_n(\mathbf{k})\rangle$, we obtain

$$W(k_1) = B^{(\mathcal{P})T}(k_1, 0) W^T(-k_1) B^{(\mathcal{P})}(k_1, 0). \quad (16)$$

Since $W(k_1)$ is periodic at k_1 , $W(k_1)$ with $k_1 = 0, \pi$ are invariant under the particle-hole operation:

$$W(k_1) = B^{(\mathcal{P})T}(k_1, 0) W^T(k_1) B^{(\mathcal{P})}(k_1, 0), \quad (k_1 = 0, \pi). \quad (17)$$

It is this invariance that protects degeneracies of Wilson loop bands at $k_1 = 0, \pi$. To see this, we parameterize the unitary matrix $W(k_1)$ as $e^{i\mathcal{H}(k_1)}$ with $\mathcal{H}(k_1)$ being a hermitian matrix periodic in k_1 , called the Wilson Hamiltonian. The eigenvalues of $\mathcal{H}(k_1)$ form the Wilson

loop bands. We can define the particle-hole operator for $\mathcal{H}(k_1)$ as $\tilde{\mathcal{P}}(k_1) = B^{(\mathcal{P})}(k_1, 0)K$ such that Eq. (16) can be written as $\mathcal{H}(k_1) = \tilde{\mathcal{P}}(-k_1)\mathcal{H}(-k_1)\tilde{\mathcal{P}}^{-1}(-k_1)$. We have $\tilde{\mathcal{P}}(k_1)\tilde{\mathcal{P}}(-k_1) = -1$ due to Eq. (12). It is worth noting that unlike the Hamiltonian $H(\mathbf{k})$ which anti-commutes with \mathcal{P} , $\mathcal{H}(k_1)$ commutes with $\tilde{\mathcal{P}}$. Because $\tilde{\mathcal{P}}^2(k_1) = -1$ and $[\tilde{\mathcal{P}}, \mathcal{H}(k_1)] = 0$ for $k_1 = 0, \pi$, the Wilson loop bands - the eigenstates of the Wilson Hamiltonian - at $k_1 = 0, \pi$ form doublets due to the Kramers theorem.

The \mathbb{Z}_2 invariant δ is defined such that $\delta = 1$ if the Wilson loop bands form a zigzag flow between $k_1 = 0$ and $k_1 = \pi$ - equivalent to a Quantum Spin Hall flow of Kramers paired Wannier centers, and $\delta = 0$ otherwise. Examples of $\delta = 1$ and $\delta = 0$ with only \mathcal{P} symmetry are shown in Figs. 3a and 3b, respectively. Fig. 3a does not contain the $C_{2z}T$ symmetry and is meant to depict the possible cases with only our anti-unitary \mathcal{P} symmetry. Because the degeneracies at $k_1 = 0, \pi$ are protected by \mathcal{P} , a zigzag flow is stable against adding \mathcal{P} -preserving bands as long as these bands are topologically trivial (they do not exhibit Wilson loop flow themselves) that do not close the gaps between the $2M$ bands and the higher/lower bands (Fig. 3a-c).

In Figs. 1e and 1g, we plot the Wilson loop bands of the middle two bands ($\epsilon_{-1}(\mathbf{k}), \epsilon_1(\mathbf{k})$) of TBG with $\theta = 1.05$ and the Wilson loop bands of the middle ten bands ($\epsilon_{-5}(\mathbf{k}) \cdots \epsilon_5(\mathbf{k})$) of TBG with $\theta = 0.7$, respectively. Both have the zigzag flow and hence have $\delta = 1$. We do not plot the Wilson loop bands of the middle ten bands of TBG with $\theta = 1.05$ because they have touching points with higher/lower bands at generic momenta (away from high symmetry lines).

B. Comparison of the \mathcal{P} -protected topology and $C_{2z}T$ -protected topology

In Ref. [58], some of the authors of the present work proved that the $C_{2z}T$ symmetry protects the Wilson loop flow for two bands, as shown in Fig. 3d, where the crossings at $\lambda = 0, \pi$ are protected by $C_{2z}T$. The Wilson loop flow is characterized by an integer-valued invariant e_2 : the winding number of a smooth branch of the Wilson loop bands. There is a gauge ambiguity for the sign of e_2 . For example, the Wilson loop bands in Fig. 3d has $e_2 = 1$ if we choose the branch going up to define the winding number and $e_2 = -1$ if we choose the branch going down. e_2 is also referred to as the Euler's class [56], as will be briefly introduced in Section V. With only $C_{2z}T$ symmetry, the flow can be broken by adding two trivial (flat) Wilson loop bands, as shown in Fig. 3d-f, since the crossings at generic positions - different from $\lambda = 0, \pi$ - in the Wilson loop spectrum are not protected by $C_{2z}T$. After the Wilson loop bands are gapped, one can still define a $C_{2z}T$ -protected \mathbb{Z}_2 invariant through the nested Wilson loop [56, 58]. Nevertheless, this $C_{2z}T$ -protected \mathbb{Z}_2 invariant does not correspond to Wannier obstruction [56, 57]. Therefore, the topology protected only by

$C_{2z}T$ is fragile. Ref. [58] showed that, by adding the unitary particle-hole symmetry \mathcal{P} , one cannot render the Stiefel-Whitney class [56] trivial by adding more bands; however, nontrivial Stiefel-Whitney index does not imply non-Wannierizable bands, and hence [58] called the index “stable”, between quotation marks; this paper removes the quotation marks by proving non-wannierizability.

On the contrary, with the \mathcal{P} symmetry, we cannot break the zigzag flow by adding trivial (non-winding) Wilson loop bands, just like in the Quantum Spin Hall problem. First, due to the Kramers degeneracy guaranteed by \mathcal{P} , a trivial state must have at least two Wilson loop bands - corresponding to the fact that, with particle-hole symmetry, we must add to the nontrivial bands, generically, two bands - of some energy $\pm E$. The two Wilson loop bands are separated at generic k_1 but degenerate at $k_1 = 0, \pi$, as shown in Fig. 3b. If we couple such a two-band trivial state to the topological state, the total Wilson loop bands are still gapless (Fig. 3c) since the degeneracies at $k_1 = 0, \pi$ are protected. Therefore, the topology protected by \mathcal{P} is stable.

If a two-band system has both $C_{2z}T$ and \mathcal{P} symmetries, the \mathbb{Z}_2 invariant protected by \mathcal{P} is given by the parity of e_2 , *i.e.*, $\delta = e_2 \bmod 2$. For example, the Wilson loop bands in Fig. 1e has $e_2 = 1$ and $\delta = 1$. There is stable topology from \mathcal{P} , in systems with an even number of bands. TBG has even number of bands (as it has to, since $\mathcal{P} = C_{2z}TP$ implies even number of bands: nonzero energy $E \neq 0$ states come in pairs $\pm E$, while zero energy states have Kramers degeneracy since $\mathcal{P}^2 = -1$); furthermore, these bands exhibit $4l + 2$ ($l \in \mathbb{N}$) Dirac nodes at zero energy (proved in Section IV), which will show that TBG is in the topologically nontrivial class of this symmetry.

C. An alternative expression of the \mathbb{Z}_2 invariant

We have mentioned that the zigzag flow of the Wilson loop bands protected by \mathcal{P} is same as the zigzag flow of Wilson loop bands protected by the time-reversal symmetry in 2D Quantum Spin Hall topological insulator [126]. Now we show that they are indeed equivalent. Suppose $H(\mathbf{k})$ have the \mathcal{P} ($\mathcal{P}^2 = -1$) symmetry, *i.e.*, $H(\mathbf{k}) = -\mathcal{P}H(-\mathbf{k})\mathcal{P}^{-1}$, then we define the squared Hamiltonian as $H^2(\mathbf{k}) = H(\mathbf{k}) \cdot H(\mathbf{k})$ such that it commutes with \mathcal{P} , *i.e.*, $H^2(\mathbf{k}) = \mathcal{P}H^2(-\mathbf{k})\mathcal{P}^{-1}$. We can regard \mathcal{P} as a “time-reversal symmetry” of $H^2(\mathbf{k})$. An eigenstate of $H(\mathbf{k})$ with the energy $\epsilon_n(\mathbf{k})$ is still an eigenstate of $H^2(\mathbf{k})$ but has the squared energy $\epsilon_n^2(\mathbf{k})$. States of the $2M$ particle-hole-symmetric bands used to define the Wilson loop (Eq. (14)), *i.e.*, $|u_{-M}(\mathbf{k})\rangle \cdots |u_M(\mathbf{k})\rangle$, form the lowest $2M$ bands of the squared Hamiltonian $H^2(\mathbf{k})$. Thus the Wilson loop operator of the $2M$ particle-hole symmetric bands of $H(\mathbf{k})$ is same as the Wilson loop operator of the $2M$ lowest bands of $H^2(\mathbf{k})$. The zigzag flow of the Wilson loop can be equivalently thought as protected by the “time-reversal symmetry” of

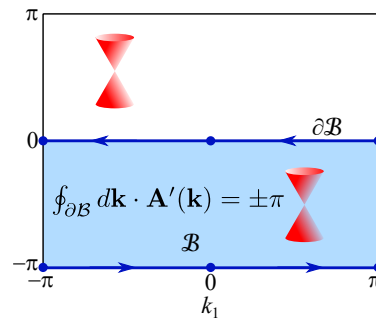


FIG. 4. The path used to define the \mathbb{Z}_2 invariant protected by \mathcal{P} . $\mathcal{B} = [-\pi, \pi] \otimes [-\pi, 0]$ is half of the Brillouin zone. Its boundary $\partial\mathcal{B}$ is invariant under the particle-hole symmetry \mathcal{P} ($\mathbf{k} \rightarrow -\mathbf{k}$). With the $C_{2z}T$ symmetry, one Dirac point in \mathcal{B} contributes to a π Berry’s phase along $\partial\mathcal{B}$.

$H^2(\mathbf{k})$.

The time-reversal-protected \mathbb{Z}_2 invariant can be alternatively expressed as a topological obstruction [128, 129]. Consider $2M$ bands $\{|u_n^I(\mathbf{k})\rangle, |u_n^{II}(\mathbf{k})\rangle | n = 1 \cdots M\}$ in a time-reversal (\mathcal{T}) symmetric system that satisfy the gauge condition $|u_n^{II}(-\mathbf{k})\rangle = \mathcal{T}|u_n^I(\mathbf{k})\rangle$, $|u_n^I(-\mathbf{k})\rangle = -\mathcal{T}|u_n^{II}(\mathbf{k})\rangle$, then the corresponding \mathbb{Z}_2 invariant is given by

$$\delta = \frac{1}{2\pi} \left(\oint_{\partial\mathcal{B}} d\mathbf{k} \cdot \mathbf{A}(\mathbf{k}) - \int_{\mathcal{B}} d^2\mathbf{k} \Omega(\mathbf{k}) \right) \bmod 2, \quad (18)$$

where \mathcal{B} is half of the BZ whose boundary $\partial\mathcal{B}$ is \mathcal{P} -invariant,

$$\mathbf{A}(\mathbf{k}) = i \sum_{n=1}^M \sum_{a=I,II} \langle u_n^a(\mathbf{k}) | \partial_{\mathbf{k}} u_n^a(\mathbf{k}) \rangle \quad (19)$$

is the Berry’s connection of the considered bands, and $\Omega(\mathbf{k}) = \partial_{\mathbf{k}} \times \mathbf{A}(\mathbf{k})$ is the Berry’s curvature. An example of \mathcal{B} is shown in Fig. 4. We regard $|u_{-M}(\mathbf{k})\rangle \cdots |u_M(\mathbf{k})\rangle$ as the lowest $2M$ bands of $H^2(\mathbf{k})$ and \mathcal{P} the “time-reversal symmetry” of $H^2(\mathbf{k})$. If we impose the gauge $|u_n(-\mathbf{k})\rangle = \mathcal{P}|u_n(\mathbf{k})\rangle$ ($n = 1 \cdots M$), *i.e.*, choose the sewing matrix defined in Eq. (11) as $B_{n',n}^{(\mathcal{P})}(\mathbf{k}) = \delta_{n',n} \text{sgn}(n)$, then we can regard $|u_n(\mathbf{k})\rangle$ and $|u_{-n}(\mathbf{k})\rangle$ as $|u_n^I(\mathbf{k})\rangle$ and $|u_n^{II}(\mathbf{k})\rangle$, respectively. Thus the \mathbb{Z}_2 invariant of the $2M$ bands of $H(\mathbf{k})$ protected by \mathcal{P} is given by Eq. (18). This expression will be used for one of the ways to prove the symmetry anomaly of $4l + 2$ Dirac points in systems with $C_{2z}T$ and \mathcal{P} symmetries (See Section IV).

IV. A no-go theorem of two Dirac fermions on lattices with $C_{2z}T$ and \mathcal{P} symmetries

In this section, we will prove that if there are $4l + 2$ ($l \in \mathbb{N}$) Dirac fermions at zero energy (chemical potential) in a system with $C_{2z}T$ and \mathcal{P} symmetries, then the \mathbb{Z}_2 invariant of the $2M$ bands (arbitrary M) above and

below the chemical potential, *i.e.*, $\epsilon_{-M}(\mathbf{k}) \cdots \epsilon_M(\mathbf{k})$, is guaranteed to be 1, provided that the $2M$ bands are gapped from other bands. As a consequence, for arbitrary M , the $2M$ particle-hole symmetric bands are not Wannierizable. That means the $4l + 2$ Dirac fermions do not have a lattice support.

Before going into a mathematical proof, we first give an intuitive proof that the Wilson loop of a $C_{2z}T$ and \mathcal{P} system with $4l + 2$ Dirac fermions at zero energy needs to wind. We first assume that we have 2 bands separate from other bands close to charge neutrality. In [48, 56] it was shown that the number of Dirac points in half BZ mod 2 equals the winding of the Wilson loop. For $4l + 2$ Dirac nodes in between these two bands, the winding would be odd, as in Fig. 1e. Adding non-trivial or nontrivial energy bands to this system would happen in pairs; introducing a set (trivial, due to $C_{2z}T$, which renders Chern numbers to be zero and hence makes any single band topologically trivial) bands at non-zero energy would have its \mathcal{P} conjugate and appear in numbers $2n$. Introducing nontrivial bands at nonzero energy would mean introducing $2 \times 2n$ bands into the system, as any possible nontrivial set of bands at a given energy comes as a multiple of 2. These bands can introduce only a multiple of 4 number of Dirac fermions into the system: each set of two separate bands has to have a multiple of 2 Dirac fermions. From our Quantum Spin Hall (QSH) experience, whatever number of bands we introduce on top of our nontrivial bands with $4l + 2$ Dirac fermions cannot change the Wilson loop winding, as we are either adding trivial bands or pairs of nontrivial bands to a QSH system. Hence the winding (of the $4n + 2$ Dirac fermion band) is stable to the addition of any bands respecting $C_{2z}T$ and \mathcal{P} . The *only* way the winding can be interrupted is by the addition of *one* set of 2 bands with Wilson loop winding to the already existent Wilson loop winding 2-bands. However, since with $C_{2z}T$ the number of Dirac nodes mod 4 is equal to twice times the winding, this additional one set of 2-bands would bring about another $4l^0 + 2$ Dirac points so the full system would have a number of Dirac fermions divisible by 4. Hence a system with $4l + 2$ Dirac fermions and $C_{2z}T$ and \mathcal{P} has to exhibit Wilson loop winding.

Now, by making use of Eq. (18), we give another proof that $2M$ bands (gapped from other bands) with $C_{2z}T$ and \mathcal{P} symmetries that have $4l + 2$ Dirac points between $\epsilon_{-1}(\mathbf{k})$ and $\epsilon_1(\mathbf{k})$ must have a nontrivial topology. Due to the $C_{2z}T$ symmetry, the Bloch states satisfy

$$C_{2z}T|u_n(\mathbf{k})\rangle = \sum_{n'} |u_{n'}(\mathbf{k})\rangle B_{n'n}^{(C_{2z}T)}(\mathbf{k}), \quad (20)$$

where $B_{n'n}^{(C_{2z}T)}(\mathbf{k})$ is unitary and called the $C_{2z}T$ sewing matrix. The summation over n^0 is limited to values satisfying $\epsilon_{n'}(\mathbf{k}) = \epsilon_n(\mathbf{k})$. Substituting this constraint into the definition of the Berry's curvature $\Omega(\mathbf{k})$, we find that $\Omega(\mathbf{k}) = 0$ [48, 56, 80]. Thus we only need to evaluate the first term on the right hand side of Eq. (18). We define $\mathbf{A}^0(\mathbf{k}) = i \sum_{n=1}^M \langle u_n(\mathbf{k}) | \partial_{\mathbf{k}} u_n(\mathbf{k}) \rangle$ for the positive bands

and $\mathbf{A}^{00}(\mathbf{k}) = i \sum_{n=1}^M \langle u_{-n}(\mathbf{k}) | \partial_{\mathbf{k}} u_{-n}(\mathbf{k}) \rangle$ for the negative bands. The total Berry's connection is $\mathbf{A} = \mathbf{A}^0 + \mathbf{A}^{00}$. By imposing the gauge condition $|u_{-n}(-\mathbf{k})\rangle = \mathcal{P}|u_n(\mathbf{k})\rangle$ ($n = 1 \cdots M$) required by Eq. (18), we find

$$\begin{aligned} \mathbf{A}''(\mathbf{k}) &= i \sum_{n=1}^M \langle u_{-n}(\mathbf{k}) | \partial_{\mathbf{k}} u_{-n}(\mathbf{k}) \rangle \\ &= i \sum_{n=1}^M \langle \partial_{\mathbf{k}} \mathcal{P} u_{-n}(\mathbf{k}) | \mathcal{P} u_{-n}(\mathbf{k}) \rangle = i \sum_{n=1}^M \langle \partial_{\mathbf{k}} u_n(-\mathbf{k}) | u_n(-\mathbf{k}) \rangle \\ &= -i \sum_{n=1}^M \langle u_n(-\mathbf{k}) | \partial_{\mathbf{k}} u_n(-\mathbf{k}) \rangle = \mathbf{A}'(-\mathbf{k}), \end{aligned} \quad (21)$$

where we have applied the property of anti-unitary symmetry introduced below Eq. (15). Since the boundary $\partial\mathcal{B}$ (Fig. 4) is invariant under $\mathbf{k} \rightarrow -\mathbf{k}$, the integrals of $\mathbf{A}^0(\mathbf{k})$ and $\mathbf{A}^{00}(\mathbf{k})$ are equal, *i.e.*,

$$\oint_{\partial\mathcal{B}} d\mathbf{k} \cdot \mathbf{A}^{00}(\mathbf{k}) = \oint_{\partial\mathcal{B}} d\mathbf{k} \cdot \mathbf{A}^0(\mathbf{k}). \quad (22)$$

The $C_{2z}T$ symmetry stabilizes 2D Dirac points [130], and each Dirac point between the positive bands and the negative bands contribute to a π or $-\pi$ Berry's phase of $\mathbf{A}^0(\mathbf{k})$ (Fig. 4). Due to the \mathcal{P} symmetry $\epsilon_{-n}(-\mathbf{k}) = -\epsilon_n(\mathbf{k})$, the Dirac points must be equally distributed in \mathcal{B} and its complementary set $\text{BZ} - \mathcal{B}$. Hence if there are $4l + 2$ Dirac points in the BZ, there will be $2l + 1$ Dirac points in \mathcal{B} and we have $\oint_{\partial\mathcal{B}} d\mathbf{k} \cdot \mathbf{A}^0(\mathbf{k}) = (2l + 1)\pi \text{ mod } 2\pi$. According to Eq. (22), we have

$$\oint_{\partial\mathcal{B}} d\mathbf{k} \cdot (\mathbf{A}^0(\mathbf{k}) + \mathbf{A}^{00}(\mathbf{k})) = (4l + 2)\pi \text{ mod } 4\pi. \quad (23)$$

Substituting this equation into Eq. (18) and using the fact that $\Omega(\mathbf{k}) = 0$, we obtain $\delta = 1$. Thus the presence of $4l + 2$ Dirac points in a system with $C_{2z}T$ and \mathcal{P} symmetries implies a nontrivial topology. In contrast to lattice models whose whole bands are trivial, this nontrivial topology is guaranteed by the Dirac points between $\epsilon_1(\mathbf{k})$ and $\epsilon_{-1}(\mathbf{k})$ and hence cannot be trivialized by adding higher and lower energy bands (preserving \mathcal{P}). Therefore, no matter how many high energy bands are included, as long as they respect $C_{2z}T$ and \mathcal{P} , the considered bands must have nontrivial topology. As will be shown in next paragraph, in a lattice model with a finite number of orbitals per unit cell, the Wilson loop bands of the whole bands must be trivial. Therefore, $4l + 2$ Dirac points cannot be realized in lattice models because the corresponding band structure, no matter how many high and low energy bands are considered, must be topologically nontrivial.

Here we show that the whole bands of a lattice model must be trivial. Let the lattice model has N orbitals, then the $U(\mathbf{k})$ matrix entering the Wilson loop operator (Eq. (14)) of the whole bands is $U(\mathbf{k}) = (|u_1(\mathbf{k})\rangle \cdots |u_N(\mathbf{k})\rangle)$. By the completeness of all the Bloch states we have $U(\mathbf{k})U^\dagger(\mathbf{k}) = 1$. Thus the Wilson loop operator in Eq. (14) is $W(k_1) =$

$U^y(k_1, 0)U(k_1, 2\pi) = U^y(k_1, 0)V^{(0, 2\pi)}U(k_1, 0)$, where $V^{(0, 2\pi)}$ is the embedding matrix defined in Appendix A (with $\mathbf{G} = 2\pi\mathbf{b}_2$). Since $U(k_1, 0)$ is an $N \times N$ unitary matrix, the eigenvalues of $W(k_1)$ are same as eigenvalues of $V^{(0, 2\pi)}$ and hence do not change with k_1 and do not wind.

It is worth noting that, in TBG, the symmetry anomaly does not depend on the parameters of the Hamiltonian Eq. (1). In the weak coupling limit ($w_0 \ll v_F k_D$, $w_1 \ll v_F k_D$), we have two Dirac points at K_M and K_M^0 in the moiré BZ. If the $2M$ bands $\epsilon_{-M}(\mathbf{k}) \cdots \epsilon_M(\mathbf{k})$ are gapped from the other bands, the $2M$ bands must be topological due to correspondence between the number of Dirac points and the \mathbb{Z}_2 invariant δ . Tuning the parameters of TBG may couple the $2M$ bands to higher bands $\epsilon_{M+1}(\mathbf{k}) \cdots \epsilon_{M'}(\mathbf{k})$ ($M^0 > M$) and lower bands $\epsilon_{-M'}(\mathbf{k}) \cdots \epsilon_{-M-1}(\mathbf{k})$, which are assumed be gapped from $\epsilon_{M'+1}(\mathbf{k})$ and $\epsilon_{-M'-1}(\mathbf{k})$ as we tune the parameters. In the weak coupling limit, the additional $2M^0 - 2M$ bands must have $\delta = 0$ since they do not have Dirac points between $\epsilon_{-M-1}(\mathbf{k})$ and $\epsilon_{M+1}(\mathbf{k})$. Therefore, after we couple the $2M$ bands to the $2M^0 - 2M$ bands, the $2M^0$ bands as a whole will have $\delta = 1 + 0 = 1$. As we tune the parameters, additional Dirac points between $\epsilon_1(\mathbf{k})$ and $\epsilon_{-1}(\mathbf{k})$ may be created due to gap closing and reopening between $\epsilon_1(\mathbf{k})$ and $\epsilon_{-1}(\mathbf{k})$. However, the total number of Dirac points between $\epsilon_1(\mathbf{k})$ and $\epsilon_{-1}(\mathbf{k})$ must equal to $2 \pmod{4}$, *i.e.*, $4l + 2$ ($l \in \mathbb{N}$), because the topological invariant of the $2M^0$ bands is guaranteed to be $\delta = 1$.

V. The Chern band basis

In this section we show that, if the two bands $\epsilon_1(\mathbf{k})$ and $\epsilon_{-1}(\mathbf{k})$ are gapped from other bands, we can recombine them as two Chern bands with Chern numbers e_2 and $-e_2$, with e_2 being the Euler's class [56, 131–133] (or, equivalently, the Wilson loop winding number protected by $C_{2z}T$ [48]). (In TBG, the Chern numbers given by $\pm e_2$ are also equal to the $e_Y = \pm 1$ index defined in Ref. [110], which, in a certain gauge, represents the eigenvalue of the Pauli y matrix in the 2-dimensional space of $n = \pm 1$ band indices.)

In order to introduce the Chern band basis, we first introduce the definition of Euler's class e_2 . (We refer the readers to Refs. [56, 131, 48] for more details.) Suppose the two bands $\epsilon_1(\mathbf{k})$ and $\epsilon_{-1}(\mathbf{k})$ are gapped from other bands. Then, at \mathbf{k} away from Dirac points between the two bands, the $C_{2z}T$ operator leaves each band unchanged up to a phase factor. In other words, the $C_{2z}T$ sewing matrix (Eq. (20)) is diagonal at these \mathbf{k} . Hence in general, the $C_{2z}T$ symmetry acts on the Bloch states as $C_{2z}T|u_n(\mathbf{k})\rangle = |u_n(\mathbf{k})\rangle e^{i\theta_n(\mathbf{k})}$ ($n = \pm 1$), with $\theta_n(\mathbf{k})$ being the phase factors. According to Ref. [56], it follows that the non-Abelian Berry's connection of the two

bands at \mathbf{k} away from Dirac points takes the form

$$\begin{aligned} \mathcal{A}_{nn'}(\mathbf{k}) &= i\langle u_n(\mathbf{k}) | \partial_{\mathbf{k}} u_{n'}(\mathbf{k}) \rangle \\ &= \begin{pmatrix} -\frac{1}{2} \partial_{\mathbf{k}} \theta_1(\mathbf{k}) & -i\mathbf{a}(\mathbf{k}) e^{i\frac{\theta_1(\mathbf{k}) - \theta_{-1}(\mathbf{k})}{2}} \\ i\mathbf{a}(\mathbf{k}) e^{i\frac{\theta_{-1}(\mathbf{k}) - \theta_1(\mathbf{k})}{2}} & -\frac{1}{2} \partial_{\mathbf{k}} \theta_{-1}(\mathbf{k}) \end{pmatrix}_{nn'}. \end{aligned} \quad (24)$$

$\mathbf{a}(\mathbf{k})$ is a gauge invariant quantity up to a global ambiguity of \pm sign. The Euler's class is given by

$$e_2 = \frac{1}{2\pi} \sum_i \oint_{\partial D_i} d\mathbf{k} \cdot \mathbf{a}(\mathbf{k}) = \frac{1}{2\pi} \int_{\text{BZ}'} d^2\mathbf{k} f(\mathbf{k}) \in \mathbb{Z}. \quad (25)$$

Here i indexes the Dirac points in the BZ, D_i is a sufficiently small region covering the i -th Dirac point, $\text{BZ}^0 = \text{BZ} - \sum_i D_i$, and $f(\mathbf{k}) = \partial_{\mathbf{k}} \times \mathbf{a}(\mathbf{k})$.

We introduce the two Chern band basis as

$$|v_{\pm}(\mathbf{k})\rangle = \frac{1}{\sqrt{2}} (e^{i\frac{\theta_1(\mathbf{k})}{2}} |u_1(\mathbf{k})\rangle \pm i e^{i\frac{\theta_{-1}(\mathbf{k})}{2}} |u_{-1}(\mathbf{k})\rangle). \quad (26)$$

There are two ambiguities in the above equation: (i) There is an ambiguity of the two branches of $\frac{\theta_n}{2}$, *i.e.*, $\frac{\theta_n}{2}$ and $\frac{\theta_n}{2} + \pi$. (ii) At the Dirac points, where the two bands are degenerate, there is an ambiguity of choosing $u_1(\mathbf{k})$ and $u_{-1}(\mathbf{k})$. Replacing $\theta_1(\mathbf{k})/2$ by $\theta_1(\mathbf{k})/2 + \pi$ or replacing $\theta_{-1}(\mathbf{k})/2$ by $\theta_{-1}(\mathbf{k})/2 + \pi$ will interchange $|v_+(\mathbf{k})\rangle$ with $|v_-(\mathbf{k})\rangle$. Similarly, interchanging $|u_1(\mathbf{k})\rangle$ and $|u_{-1}(\mathbf{k})\rangle$ at the Dirac points will also interchange $|v_+(\mathbf{k})\rangle$ with $|v_-(\mathbf{k})\rangle$ at the Dirac points. To solve these ambiguities, as detailed in Appendix B, we require that the Berry's curvatures of $|v_+(\mathbf{k})\rangle$ and $|v_-(\mathbf{k})\rangle$ to be continuous, or, equivalently,

$$\lim_{\mathbf{q} \rightarrow 0} |\langle v_{m'}(\mathbf{k} + \mathbf{q}) | v_m(\mathbf{k}) \rangle| = \delta_{m'm}, \quad (27)$$

where $m, m^0 = \pm$. Using Eqs. (24) and (26), we can calculate the non-Abelian Berry's connection on the basis $|v_{\pm}(\mathbf{k})\rangle$ at \mathbf{k} away from the Dirac points. We obtain

$$\mathcal{A}_{mm'}^0(\mathbf{k}) = i\langle v_m(\mathbf{k}) | \partial_{\mathbf{k}} v_{m'}(\mathbf{k}) \rangle = \begin{pmatrix} \mathbf{a}(\mathbf{k}) & 0 \\ 0 & -\mathbf{a}(\mathbf{k}) \end{pmatrix}_{mm'}, \quad (28)$$

and hence

$$\mathcal{F}_{mm'}^0 = -[\partial_{k_x} - \mathcal{A}_x^0, \partial_{k_y} - \mathcal{A}_y^0]_{mm'} = \begin{pmatrix} f(\mathbf{k}) & 0 \\ 0 & -f(\mathbf{k}) \end{pmatrix}_{mm'}, \quad (29)$$

for \mathbf{k} not at the Dirac points. Therefore, if the Berry's curvature does not diverge at Dirac points, which is true as shown in next paragraph, the Chern numbers of the states $|v_{\pm}(\mathbf{k})\rangle$ are

$$C_{\pm} = \pm \frac{1}{2\pi} \int d^2\mathbf{k} f(\mathbf{k}) = \pm e_2. \quad (30)$$

To conclude this section, we show that in the chiral limit $w_0 = 0$ the Chern band basis can be chosen as the eigenstates of the chiral symmetry C (Eq. (7)). We define the sewing matrix of C as

$$C|u_n(\mathbf{k})\rangle = \sum_{n'} |u_{n'}(\mathbf{k})\rangle B_{n'n}^{(C)}(\mathbf{k}), \quad (31)$$

where the summation over n^0 satisfies $\epsilon_{n'}(\mathbf{k}) = -\epsilon_n(\mathbf{k})$. For the TBG Hamiltonian Eq. (1), the $C_{2z}T$ and C operators are $\sigma_x K$ and σ_z , respectively. Thus we have the algebra $C^2 = 1$ and $\{C, C_{2z}T\} = 0$ and hence

$$[B^{(C)}(\mathbf{k})]^2 = 1, \quad (32)$$

$$B^{(C_{2z}T)}(\mathbf{k})B^{(C)}(\mathbf{k}) + B^{(C)}(\mathbf{k})B^{(C_{2z}T)}(\mathbf{k}) = 0. \quad (33)$$

As discussed at the beginning of this section, at \mathbf{k} not at the Dirac points, we have $B_{n'n}^{(C_{2z}T)}(\mathbf{k}) = \delta_{n'n}e^{i\theta_n(\mathbf{k})}$. Then the solution of $B^{(C)}(\mathbf{k})$ is

$$B^{(C)}(\mathbf{k}) = \pm \begin{pmatrix} 0 & -ie^{i\frac{\theta_1(\mathbf{k}) - \theta_{-1}(\mathbf{k})}{2}} \\ ie^{i\frac{\theta_{-1}(\mathbf{k}) - \theta_1(\mathbf{k})}{2}} & 0 \end{pmatrix}. \quad (34)$$

The \pm sign cannot be determined by solving Eqs. (32) and (33). In practice, one should evaluate Eq. (31) to determine the \pm sign for given $|u_{\pm}(\mathbf{k})\rangle$. We find that the Chern band basis Eq. (26) diagonalizes $B^{(C)}(\mathbf{k})$. Below Eq. (26) we have discussed the ambiguity of choosing $|v_{\pm}(\mathbf{k})\rangle$ and we have imposed Eq. (27) to fix this ambiguity. This ambiguity of Eq. (26) can be alternatively solved by choosing $|v_{\pm}(\mathbf{k})\rangle$ as the eigenstates of C with the eigenvalues ± 1 , respectively. This choice automatically satisfies Eq. (27) since the states with different chiral eigenvalues are orthogonal, *i.e.*, $\langle v_{\pm}(\mathbf{k}) | v_{\pm}(\mathbf{k}^0) \rangle = \langle v_{\pm}(\mathbf{k}) | C^y C | v_{\pm}(\mathbf{k}^0) \rangle = -\langle v_{\pm}(\mathbf{k}) | v_{\pm}(\mathbf{k}^0) \rangle = 0$ for arbitrary \mathbf{k} and \mathbf{k}^0 .

The Chern band basis in Eq. (26) can also be equivalently defined through the Wilson loop method [86]. Besides, in the chiral limit, the Chern band basis we defined is equivalent to that defined in [23].

VI. Perfect metal phase of twisted bilayer graphene in the second chiral limit

In our article Ref. [110], we consider the opposite limit of the usual chiral limit: Instead of letting $w_0 = 0$, we take w_1 to be zero. When $w_1 = 0$, the model Eq. (1) has another chiral symmetry $C^0 = \tau_z \sigma_z$ acting on the Hamiltonian as $C^0 H(\mathbf{r}) C^{0y} = -H(\mathbf{r})$. Thus we call this limit as the second chiral limit. As discussed in Section II A, w_0 and w_1 are the interlayer couplings contributed mainly by the AA and AB/BA regions, respectively; thus the second chiral limit can be (approximately) realized if the layer distance in the AA region is smaller than the layer distance in the AB and BA regions (shorter distance means stronger coupling). Such a configuration would be different from the corrugation predicted by the first principle calculations [119–122], where the distance in the AA region is larger. Nevertheless, the second chiral limit might could potentially be engineered by putting the TBG on certain substrate, and it represents an interesting interacting limit [110]. We are mainly interested in the novel electronic band structure of TBG in the second

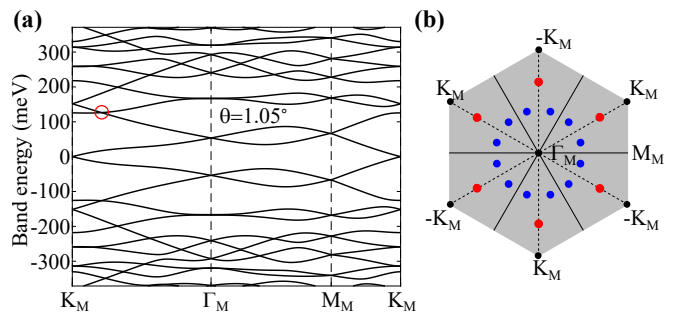


FIG. 5. Perfect metal phase of twisted bilayer graphene in the second chiral limit ($w_1 = 0$). (a) The band structure at $\theta = 1.05^\circ$ with the parameters $v_F = 5.944\text{eV} \cdot \text{\AA}$, $|K| = 1.703\text{\AA}^{-1}$, $w_1 = 0$, $w_0 = 77\text{meV}$. (b) The Brillouin zone of the twisted bilayer graphene. The solid black lines represent the C_{2x} -axis and its conjugations under C_{3z} , the dashed black lines represent the effective mirror symmetry $M_x = C_{2x}I$ and its conjugations under C_{3z} . The red dots represent Dirac points in the mirror lines. The blue dots represent Dirac points at generic momenta.

chiral limit and hence we leave the material realization of the second chiral limit for future study.

We find that, in the second chiral limit, the n -th positive (negative) band is always connected to the $(n+1)$ -th positive (negative) band. As the first positive band and the first negative band are connected through the Dirac points, the *whole* bands are all connected, as shown in Fig. 5a. The phase with all bands connected is referred to as the perfect metal [134] in trilayer systems, where the number of Dirac nodes is odd. In the current case, we also find this “perfect metal” in even number of Dirac node systems with the special chiral symmetry of the second chiral limit.

The perfect metal phase is protected by $C_{2z}T$, P , and C^0 . The new chiral symmetry C^0 has a strange group algebra as it anticommutes with T and with P [111]. We define the product of P and C^0 as an effective inversion symmetry $I = PC^0 = \tau_x \sigma_z$. It commutes with the Hamiltonian, *i.e.*, $H(-\mathbf{r}) = IH(\mathbf{r})I^y$ and $H(-\mathbf{k}) = IH(\mathbf{k})I^y$ accordingly. The effective inversion operator satisfies the algebra

$$\{C_{2z}T, I\} = 0, \quad \{P, I\} = 0, \quad I^2 = 1. \quad (35)$$

We first show that $C_{2z}T$ and I protect double degeneracies at I -invariant momenta. (In TBG, the I -invariant momenta are Γ_M and the three equivalent M_M .) Since the Hamiltonian at an I -invariant momentum commutes with I , the Bloch states at this momentum must form eigenstates of I . Suppose $|u\rangle$ is such an eigenstate with I eigenvalue 1, then we can show that $C_{2z}T|u\rangle$ must have the opposite I eigenvalue -1 due to the anti-commutation between $C_{2z}T$ and I . Therefore $|u\rangle$ and $C_{2z}T|u\rangle$ form a doublet that has opposite I eigenvalues. This explains the double degeneracies at Γ_M and M_M shown in Fig. 5a.

Next we prove that, for arbitrary even M , the M -th positive band is connected to the $(M+1)$ -th positive

bands through $4l + 2$ ($l \in \mathbb{N}$) Dirac points. (For odd M , we know by counting - see Fig. 5 - that the M -th band is connected to the $(M + 1)$ -th band through the double degeneracies at the I -invariant momenta.) We only need to prove for the situation where the four bands $\epsilon_{M-1}(\mathbf{k})$, $\epsilon_M(\mathbf{k})$, $\epsilon_{M+1}(\mathbf{k})$, $\epsilon_{M+2}(\mathbf{k})$ do *not* form four-fold degeneracies at high symmetry momenta since otherwise $\epsilon_M(\mathbf{k})$ is already connected to $\epsilon_{M+1}(\mathbf{k})$. (As shown in Fig. 5a, we also do not observe four-fold degeneracies at high symmetry momenta.) We assume there are in total n_D Dirac points between the first M positive bands $\epsilon_1(\mathbf{k}) \cdots \epsilon_M(\mathbf{k})$ and the other bands. The n_D Dirac points can appear above the M -th band, *i.e.*, between $\epsilon_M(\mathbf{k})$ and $\epsilon_{M+1}(\mathbf{k})$, or below the first band, *i.e.*, between $\epsilon_1(\mathbf{k})$ and $\epsilon_{-1}(\mathbf{k})$. According to the I symmetry, half of the BZ (\mathcal{B}) must have $n_D/2$ Dirac points. (The choice of \mathcal{B} is not unique. An example is shown in Fig. 4.) With the $C_{2z}T$ symmetry, the number of Dirac points in \mathcal{B} is related to the Berry's phase surrounding \mathcal{B} as [130]

$$\frac{n_D}{2} = \frac{1}{\pi} \oint_{\partial\mathcal{B}} d\mathbf{k} \cdot \mathbf{A}^0(\mathbf{k}) \pmod{2}, \quad (36)$$

where $\mathbf{A}^0(\mathbf{k}) = \sum_{n=1}^M i \langle u_n(\mathbf{k}) | \partial_{\mathbf{k}} u_n(\mathbf{k}) \rangle$ is the Berry's connection of the first M positive bands. In presence of the effective inversion symmetry I , the right hand side of the above equation is determined by the I eigenvalues as [127, 135–137]

$$\exp\left(i \oint_{\partial\mathcal{B}} d\mathbf{k} \cdot \mathbf{A}^0(\mathbf{k})\right) = \prod_{\mathcal{K}} \prod_{n=1}^M \xi_{\mathcal{K},n}, \quad (37)$$

where \mathcal{K} indexes the four I -invariant momenta, and $\xi_{\mathcal{K},n}$ is the I eigenvalue of the n -th positive band at the momentum \mathcal{K} . As discussed in the last paragraph, each doublet at an I -invariant momentum has opposite I eigenvalues. Thus, there are equal number of I eigenvalues 1 and -1 at the I -invariant momenta; since the total number of states at the four I -invariant momenta is $4M$, there are $2M$ eigenvalues with $I = +1$ and $2M$ eigenvalues with $I = -1$. Hence the right hand side of Eq. (37) is 1 and we have $\oint_{\partial\mathcal{B}} d\mathbf{k} \cdot \mathbf{A}^0(\mathbf{k}) = 0 \pmod{2\pi}$. According to Eq. (36), the total number of Dirac points is a multiple of 4, *i.e.*, $n_D = 0 \pmod{4}$. As we have proved in Section IV, there must be $4l^0 + 2$ ($l^0 \in \mathbb{N}$) Dirac points between $\epsilon_1(\mathbf{k})$ and $\epsilon_{-1}(\mathbf{k})$, then the number of Dirac points between $\epsilon_M(\mathbf{k})$ and $\epsilon_{M+1}(\mathbf{k})$ is $n_D - 4l^0 - 2 = 4l + 2$ with $l = n_D/4 - l^0 - 1 \in \mathbb{N}$. Thus the M -th positive band is always connected to the $(M + 1)$ -th positive band through $4l + 2$ Dirac points. According to the particle-hole symmetry P , the M -th negative band is also connected to the $(M + 1)$ -th negative band through $4l + 2$ Dirac points. Therefore, the whole set of bands in the system will be connected.

In general, the $4l + 2$ Dirac points between the M -th band and the $(M + 1)$ -th band can be located anywhere in the BZ. However, with the C_{3z} and the C_{2x} symmetries of TBG, at least some of the $4l + 2$ Dirac points must locate

at high symmetry point or along high symmetry lines of the BZ. We prove this statement by contradiction. The unitary point group of TBG is generated by C_{3z} , C_{2x} , and the effective inversion I and hence is isomorphic to the point group D_{3d} , which has 12 elements in total. If all the Dirac points between the M -th band and the $(M + 1)$ -th band are located at generic momenta, then the number of Dirac points would be a multiple of 12, as represented by the blue dots in Fig. 5b, leading to a contradiction with the $4l + 2$ Dirac points. Therefore, there must be 2 (modulo 4) Dirac points at the high symmetry points or along the high symmetry lines. As a consequence, the entire set of bands of TBG in the second chiral limit must be connected along the high symmetry lines. For example, as shown in Fig. 5a, there is a crossing between the 2nd and 3rd bands in the high symmetry line $\Gamma_M - K_M$. (This crossing is protected by the effective mirror symmetry $M_x = C_{2x}I$.) Under the actions of C_{2x} and C_{3z} , there are in total six symmetry counterparts of this crossing point (including itself). Thus the number of Dirac points is consistent with $4l + 2$ with $l = 1$.

VII. Conclusions

In this work, we showed that even the simple, well studied BM TBG model still has several surprises related to the deep physics that it describes. We have proved that the band structure in a single graphene valley of TBG is anomalous, *i.e.*, does not have lattice support that respects the $C_{2z}T$ and \mathcal{P} symmetries. The anomaly manifests as (i) a \mathbb{Z}_2 nontrivial topology protected \mathcal{P} of the $2M$ bands $\epsilon_{-M}(\mathbf{k}) \cdots \epsilon_M(\mathbf{k})$ for arbitrary M , provided that the $2M$ bands are gapped from other bands, (ii) $4l + 2$ ($l \in \mathbb{N}$) Dirac points between $\epsilon_{-1}(\mathbf{k})$ and $\epsilon_1(\mathbf{k})$. In the second chiral limit ($w_1 = 0$), the anomaly manifests as (iii) a perfect metal phase where all the bands are connected.

As a consequence of the symmetry anomaly, a faithful description of TBG that respects all the symmetries of TBG, including \mathcal{P} , is *forced to* adopt a momentum space formalism. Any tight-binding description [1, 2, 23, 57, 66] of TBG with finite number of orbitals must break at least one of the $C_{2z}T$ and \mathcal{P} symmetries (or the valley symmetry if the tight-binding model mix the two graphene valleys of TBG). In the other works of our series on TBG [109–113], the interacting physics is studied using a momentum space formalism.

Acknowledgments

We thank Aditya Cowsik and Fang Xie for valuable discussions. This work was supported by the DOE Grant No. DE-SC0016239, the Schmidt Fund for Innovative Research, Simons Investigator Grant No. 404513, the Packard Foundation, the Gordon and Betty Moore Foundation through Grant No. GBMF8685 towards the

Princeton theory program, and a Guggenheim Fellowship from the John Simon Guggenheim Memorial Foundation. Further support was provided by the NSF-EAGER No. DMR 1643312, NSF-MRSEC No. DMR-1420541 and DMR-2011750, ONR No. N00014-20-1-2303, Gordon and

Betty Moore Foundation through Grant GBMF8685 towards the Princeton theory program, BSF Israel US foundation No. 2018226, and the Princeton Global Network Funds.

-
- [1] Jian Kang and Oskar Vafek. Symmetry, Maximally Localized Wannier States, and a Low-Energy Model for Twisted Bilayer Graphene Narrow Bands. *Phys. Rev. X*, 8(3):031088, 2018.
- [2] Mikito Koshino, Noah F. Q. Yuan, Takashi Koretsune, Masayuki Ochi, Kazuhiko Kuroki, and Liang Fu. Maximally localized wannier orbitals and the extended hubbard model for twisted bilayer graphene. *Phys. Rev. X*, 8:031087, Sep 2018.
- [3] Jianpeng Liu, Junwei Liu, and Xi Dai. Pseudo landau level representation of twisted bilayer graphene: Band topology and implications on the correlated insulating phase. *Physical Review B*, 99(15):155415, 2019.
- [4] Liujun Zou, Hoi Chun Po, Ashvin Vishwanath, and T. Senthil. Band structure of twisted bilayer graphene: Emergent symmetries, commensurate approximants, and wannier obstructions. *Phys. Rev. B*, 98:085435, Aug 2018.
- [5] Rafi Bistritzer and Allan H. MacDonald. Moiré bands in twisted double-layer graphene. *Proceedings of the National Academy of Sciences*, 108(30):12233–12237, July 2011.
- [6] Yuan Cao, Valla Fatemi, Ahmet Demir, Shiang Fang, Spencer L. Tomarken, Jason Y. Luo, Javier D. Sanchez-Yamagishi, Kenji Watanabe, Takashi Taniguchi, Efthimios Kaxiras, Ray C. Ashoori, and Pablo Jarillo-Herrero. Correlated insulator behaviour at half-filling in magic-angle graphene superlattices. *Nature*, 556(7699):80–84, April 2018.
- [7] Dmitry K. Efimkin and Allan H. MacDonald. Helical network model for twisted bilayer graphene. *Phys. Rev. B*, 98:035404, Jul 2018.
- [8] Yonglong Xie, Biao Lian, Berthold Jäck, Xiaomeng Liu, Cheng-Li Chiu, Kenji Watanabe, Takashi Taniguchi, B Andrei Bernevig, and Ali Yazdani. Spectroscopic signatures of many-body correlations in magic-angle twisted bilayer graphene. *Nature*, 572(7767):101–105, 2019.
- [9] Ipsita Das, Xiaobo Lu, Jonah Herzog-Arbeitman, Zhi-Da Song, Kenji Watanabe, Takashi Taniguchi, B Andrei Bernevig, and Dmitri K Efetov. Symmetry broken chern insulators and magic series of rashba-like landau level crossings in magic angle bilayer graphene. *arXiv preprint arXiv:2007.13390*, 2020.
- [10] Hoi Chun Po, Liujun Zou, Ashvin Vishwanath, and T. Senthil. Origin of Mott Insulating Behavior and Superconductivity in Twisted Bilayer Graphene. *Physical Review X*, 8(3):031089, September 2018.
- [11] John F Dodaro, Steven A Kivelson, Yoni Schattner, Xiao-Qi Sun, and Chao Wang. Phases of a phenomenological model of twisted bilayer graphene. *Physical Review B*, 98(7):075154, 2018.
- [12] Noah FQ Yuan and Liang Fu. Model for the metal-insulator transition in graphene superlattices and beyond. *Physical Review B*, 98(4):045103, 2018.
- [13] Masayuki Ochi, Mikito Koshino, and Kazuhiko Kuroki. Possible correlated insulating states in magic-angle twisted bilayer graphene under strongly competing interactions. *Phys. Rev. B*, 98:081102, Aug 2018.
- [14] Xiao Yan Xu, K. T. Law, and Patrick A. Lee. Kekulé valence bond order in an extended hubbard model on the honeycomb lattice with possible applications to twisted bilayer graphene. *Phys. Rev. B*, 98:121406, Sep 2018.
- [15] Jörn W. F. Venderbos and Rafael M. Fernandes. Correlations and electronic order in a two-orbital honeycomb lattice model for twisted bilayer graphene. *Phys. Rev. B*, 98:245103, Dec 2018.
- [16] Jian Kang and Oskar Vafek. Strong Coupling Phases of Partially Filled Twisted Bilayer Graphene Narrow Bands. *Physical Review Letters*, 122(24):246401, June 2019.
- [17] Jianpeng Liu, Zhen Ma, Jinhua Gao, and Xi Dai. Quantum valley hall effect, orbital magnetism, and anomalous hall effect in twisted multilayer graphene systems. *Physical Review X*, 9(3):031021, 2019.
- [18] Yuhang Jiang, Xinyuan Lai, Kenji Watanabe, Takashi Taniguchi, Kristjan Haule, Jinhai Mao, and Eva Y. Andrei. Charge order and broken rotational symmetry in magic-angle twisted bilayer graphene. *Nature*, 573(7772):91–95, Jul 2019.
- [19] Youngjoon Choi, Jeannette Kemmer, Yang Peng, Alex Thomson, Harpreet Arora, Robert Polski, Yiran Zhang, Hechen Ren, Jason Alicea, Gil Refael, and et al. Electronic correlations in twisted bilayer graphene near the magic angle. *Nature Physics*, 15(11):1174–1180, Aug 2019.
- [20] Hryhoriy Polshyn, Matthew Yankowitz, Shaowen Chen, Yuxuan Zhang, K. Watanabe, T. Taniguchi, Cory R. Dean, and Andrea F. Young. Large linear-in-temperature resistivity in twisted bilayer graphene. *Nature Physics*, 15(10):1011–1016, Aug 2019.
- [21] Jed H. Pixley and Eva Y. Andrei. Ferromagnetism in magic-angle graphene. *Science*, 365(6453):543–543, 2019.
- [22] Ming Xie and A. H. MacDonald. Nature of the correlated insulator states in twisted bilayer graphene. *Phys. Rev. Lett.*, 124:097601, Mar 2020.
- [23] Nick Bultinck, Eslam Khalaf, Shang Liu, Shubhayu Chatterjee, Ashvin Vishwanath, and Michael P. Zaletel. Ground state and hidden symmetry of magic-angle graphene at even integer filling. *Phys. Rev. X*, 10:031034, Aug 2020.
- [24] Kevin P. Nuckolls, Myungchul Oh, Dillon Wong, Biao Lian, Kenji Watanabe, Takashi Taniguchi, B. Andrei Bernevig, and Ali Yazdani. Strongly Correlated Chern Insulators in Magic-Angle Twisted Bilayer Graphene. *arXiv e-prints*, page arXiv:2007.03810, July 2020.
- [25] Shuang Wu, Zhenyuan Zhang, K. Watanabe,

- T. Taniguchi, and Eva Y. Andrei. Chern Insulators and Topological Flat-bands in Magic-angle Twisted Bilayer Graphene. *arXiv e-prints*, page arXiv:2007.03735, July 2020.
- [26] Yu Saito, Jingyuan Ge, Louk Rademaker, Kenji Watanabe, Takashi Taniguchi, Dmitry A. Abanin, and Andrea F. Young. Hofstadter subband ferromagnetism and symmetry broken Chern insulators in twisted bilayer graphene. *arXiv e-prints*, page arXiv:2007.06115, July 2020.
- [27] Dillon Wong, Kevin P. Nuckolls, Myungchul Oh, Biao Lian, Yonglong Xie, Sangjun Jeon, Kenji Watanabe, Takashi Taniguchi, B. Andrei Bernevig, and Ali Yazdani. Cascade of electronic transitions in magic-angle twisted bilayer graphene. *Nature*, 582(7811):198–202, Jun 2020.
- [28] U. Zondiner, A. Rozen, D. Rodan-Legrain, Y. Cao, R. Queiroz, T. Taniguchi, K. Watanabe, Y. Oreg, F. von Oppen, Ady Stern, and et al. Cascade of phase transitions and dirac revivals in magic-angle graphene. *Nature*, 582(7811):203–208, Jun 2020.
- [29] Aaron L. Sharpe, Eli J. Fox, Arthur W. Barnard, Joe Finney, Kenji Watanabe, Takashi Taniguchi, M. A. Kastner, and David Goldhaber-Gordon. Emergent ferromagnetism near three-quarters filling in twisted bilayer graphene. *Science*, 365(6453):605–608, Jul 2019.
- [30] M. Serlin, C. L. Tschirhart, H. Polshyn, Y. Zhang, J. Zhu, K. Watanabe, T. Taniguchi, L. Balents, and A. F. Young. Intrinsic quantized anomalous hall effect in a moiré heterostructure. *Science*, 367(6480):900–903, Dec 2019.
- [31] Nick Bultinck, Shubhayu Chatterjee, and Michael P. Zaletel. Mechanism for anomalous hall ferromagnetism in twisted bilayer graphene. *Phys. Rev. Lett.*, 124:166601, Apr 2020.
- [32] Yu Saito, Jingyuan Ge, Kenji Watanabe, Takashi Taniguchi, Erez Berg, and Andrea F. Young. Isospin pomeranchuk effect and the entropy of collective excitations in twisted bilayer graphene, 2020.
- [33] Jian Kang and Oskar Vafek. Non-abelian dirac node braiding and near-degeneracy of correlated phases at odd integer filling in magic-angle twisted bilayer graphene. *Phys. Rev. B*, 102:035161, Jul 2020.
- [34] Tomohiro Soejima, Daniel E. Parker, Nick Bultinck, Johannes Hauschild, and Michael P. Zaletel. Efficient simulation of moire materials using the density matrix renormalization group, 2020.
- [35] Yuan Cao, Debanjan Chowdhury, Daniel Rodan-Legrain, Oriol Rubies-Bigorda, Kenji Watanabe, Takashi Taniguchi, T. Senthil, and Pablo Jarillo-Herrero. Strange metal in magic-angle graphene with near planckian dissipation. *Phys. Rev. Lett.*, 124:076801, Feb 2020.
- [36] Yves H. Kwan, Glenn Wagner, Nilotpal Chakraborty, Steven H. Simon, and S. A. Parameswaran. Orbital chern insulator domain walls and chiral modes in twisted bilayer graphene, 2020.
- [37] Yuan Cao, Valla Fatemi, Shiang Fang, Kenji Watanabe, Takashi Taniguchi, Efthimios Kaxiras, and Pablo Jarillo-Herrero. Unconventional superconductivity in magic-angle graphene superlattices. *Nature*, 556(7699):43–50, April 2018.
- [38] Xiaobo Lu, Petr Stepanov, Wei Yang, Ming Xie, Mohammed Ali Aamir, Ipsita Das, Carles Urgell, Kenji Watanabe, Takashi Taniguchi, Guangyu Zhang, et al. Superconductors, orbital magnets and correlated states in magic-angle bilayer graphene. *Nature*, 574(7780):653–657, 2019.
- [39] Matthew Yankowitz, Shaowen Chen, Hryhoriy Polshyn, Yuxuan Zhang, K Watanabe, T Taniguchi, David Graf, Andrea F Young, and Cory R Dean. Tuning superconductivity in twisted bilayer graphene. *Science*, 363(6431):1059–1064, 2019.
- [40] Fengcheng Wu, A. H. MacDonald, and Ivar Martin. Theory of phonon-mediated superconductivity in twisted bilayer graphene. *Phys. Rev. Lett.*, 121:257001, Dec 2018.
- [41] Cenke Xu and Leon Balents. Topological superconductivity in twisted multilayer graphene. *Physical review letters*, 121(8):087001, 2018.
- [42] Cheng-Cheng Liu, Li-Da Zhang, Wei-Qiang Chen, and Fan Yang. Chiral spin density wave and d+id superconductivity in the magic-angle-twisted bilayer graphene. *Physical review letters*, 121(21):217001, 2018.
- [43] Hiroki Isobe, Noah FQ Yuan, and Liang Fu. Unconventional superconductivity and density waves in twisted bilayer graphene. *Physical Review X*, 8(4):041041, 2018.
- [44] Francisco Guinea and Niels R. Walet. Electrostatic effects, band distortions, and superconductivity in twisted graphene bilayers. *Proceedings of the National Academy of Sciences*, 115(52):13174–13179, 2018.
- [45] Jose Gonzalez and Tobias Stauber. Kohn-luttinger superconductivity in twisted bilayer graphene. *Physical review letters*, 122(2):026801, 2019.
- [46] Biao Lian, Zhijun Wang, and B. Andrei Bernevig. Twisted bilayer graphene: A phonon-driven superconductor. *Phys. Rev. Lett.*, 122:257002, Jun 2019.
- [47] Y.-Z. You and A. Vishwanath. Superconductivity from Valley Fluctuations and Approximate SO(4) Symmetry in a Weak Coupling Theory of Twisted Bilayer Graphene. *npj Quantum Materials*, 4:16, Apr 2019.
- [48] Fang Xie, Zhida Song, Biao Lian, and B. Andrei Bernevig. Topology-bounded superfluid weight in twisted bilayer graphene. *Phys. Rev. Lett.*, 124:167002, Apr 2020.
- [49] Yu Saito, Jingyuan Ge, Kenji Watanabe, Takashi Taniguchi, and Andrea F. Young. Independent superconductors and correlated insulators in twisted bilayer graphene. *Nature Physics*, 16(9):926–930, Jun 2020.
- [50] Petr Stepanov, Ipsita Das, Xiaobo Lu, Ali Fahimniya, Kenji Watanabe, Takashi Taniguchi, Frank H. L. Koppens, Johannes Lischner, Leonid Levitov, and Dmitri K. Efetov. Untying the insulating and superconducting orders in magic-angle graphene. *Nature*, 583(7816):375–378, Jul 2020.
- [51] Harpreet Singh Arora, Robert Polski, Yiran Zhang, Alex Thomson, Youngjoon Choi, Hyunjin Kim, Zhong Lin, Ilham Zaky Wilson, Xiaodong Xu, Jiun-Haw Chu, and et al. Superconductivity in metallic twisted bilayer graphene stabilized by wse2. *Nature*, 583(7816):379–384, Jul 2020.
- [52] Eslam Khalaf, Shubhayu Chatterjee, Nick Bultinck, Michael P. Zaletel, and Ashvin Vishwanath. Charged skyrmions and topological origin of superconductivity in magic angle graphene, 2020.
- [53] Fengcheng Wu and Sankar Das Sarma. Collective excitations of quantum anomalous hall ferromagnets in twisted bilayer graphene. *Physical Review Letters*,

- 124(4), Jan 2020.
- [54] A. Julku, T. J. Peltonen, L. Liang, T. T. Heikkilä, and P. Törmä. Superfluid weight and berezinskii-kosterlitz-thouless transition temperature of twisted bilayer graphene. *Physical Review B*, 101(6), Feb 2020.
- [55] E. J. König, Piers Coleman, and A. M. Tsvelik. Spin magnetometry as a probe of stripe superconductivity in twisted bilayer graphene, 2020.
- [56] Junyeong Ahn, Sungjoon Park, and Bohm-Jung Yang. Failure of Nielsen-Ninomiya Theorem and Fragile Topology in Two-Dimensional Systems with Space-Time Inversion Symmetry: Application to Twisted Bilayer Graphene at Magic Angle. *Physical Review X*, 9(2):021013, April 2019.
- [57] Hoi Chun Po, LiuJun Zou, T. Senthil, and Ashvin Vishwanath. Faithful tight-binding models and fragile topology of magic-angle bilayer graphene. *Physical Review B*, 99(19):195455, May 2019.
- [58] Zhida Song, Zhijun Wang, Wujun Shi, Gang Li, Chen Fang, and B. Andrei Bernevig. All Magic Angles in Twisted Bilayer Graphene are Topological. *Physical Review Letters*, 123(3):036401, July 2019.
- [59] Grigory Tarnopolsky, Alex Jura Kruchkov, and Ashvin Vishwanath. Origin of Magic Angles in Twisted Bilayer Graphene. *Physical Review Letters*, 122(10):106405, March 2019.
- [60] Yixing Fu, E. J. König, J. H. Wilson, Yang-Zhi Chou, and J. H. Pixley. Magic-angle semimetals, 2018.
- [61] Ya-Hui Zhang, Dan Mao, Yuan Cao, Pablo Jarillo-Herrero, and T Senthil. Nearly flat chern bands in moiré superlattices. *Physical Review B*, 99(7):075127, 2019.
- [62] Biao Lian, Fang Xie, and B. Andrei Bernevig. Landau level of fragile topology. *Phys. Rev. B*, 102:041402, Jul 2020.
- [63] Xiaobo Lu, Biao Lian, Gaurav Chaudhary, Benjamin A. Piot, Giulio Romagnoli, Kenji Watanabe, Takashi Taniguchi, Martino Poggio, Allan H. MacDonald, B. Andrei Bernevig, and Dmitri K. Efetov. Fingerprints of fragile topology in the hofstadter spectrum of twisted bilayer graphene close to the second magic angle, 2020.
- [64] Bikash Padhi, Apoorv Tiwari, Titus Neupert, and Shinsei Ryu. Transport across twist angle domains in moiré graphene, 2020.
- [65] Jonah Herzog-Arbeitman, Zhi-Da Song, Nicolas Regnault, and B. Andrei Bernevig. Hofstadter Topology: Non-crystalline Topological Materials in the Moiré Era. *arXiv:2006.13938 [cond-mat]*, June 2020. arXiv: 2006.13938.
- [66] Justin H. Wilson, Yixing Fu, S. Das Sarma, and J. H. Pixley. Disorder in twisted bilayer graphene. *Phys. Rev. Research*, 2:023325, Jun 2020.
- [67] Xiaoxue Liu, Zhi Wang, K Watanabe, T Taniguchi, Oskar Vafek, and JIA Li. Tuning electron correlation in magic-angle twisted bilayer graphene using coulomb screening. *arXiv preprint arXiv:2003.11072*, 2020.
- [68] Alexander Kerelsky, Leo J. McGilly, Dante M. Kennes, Lede Xian, Matthew Yankowitz, Shaowen Chen, K. Watanabe, T. Taniguchi, James Hone, Cory Dean, and et al. Maximized electron interactions at the magic angle in twisted bilayer graphene. *Nature*, 572(7767):95–100, Jul 2019.
- [69] Youngjoon Choi, Hyunjin Kim, Yang Peng, Alex Thomson, Cyprian Lewandowski, Robert Polski, Yiran Zhang, Harpreet Singh Arora, Kenji Watanabe, Takashi Taniguchi, Jason Alicea, and Stevan Nadj-Perge. Tracing out correlated chern insulators in magic angle twisted bilayer graphene, 2020.
- [70] Jeong Min Park, Yuan Cao, Kenji Watanabe, Takashi Taniguchi, and Pablo Jarillo-Herrero. Flavour hund’s coupling, correlated chern gaps, and diffusivity in moiré flat bands, 2020.
- [71] Asaf Rozen, Jeong Min Park, Uri Zondiner, Yuan Cao, Daniel Rodan-Legrain, Takashi Taniguchi, Kenji Watanabe, Yuval Oreg, Ady Stern, Erez Berg, Pablo Jarillo-Herrero, and Shahal Ilani. Entropic evidence for a pomeranchuk effect in magic angle graphene, 2020.
- [72] G. William Burg, Jihang Zhu, Takashi Taniguchi, Kenji Watanabe, Allan H. MacDonald, and Emanuel Tutuc. Correlated insulating states in twisted double bilayer graphene. *Phys. Rev. Lett.*, 123:197702, Nov 2019.
- [73] Cheng Shen, Yanbang Chu, QuanSheng Wu, Na Li, Shuopei Wang, Yanchong Zhao, Jian Tang, Jieying Liu, Jinpeng Tian, Kenji Watanabe, Takashi Taniguchi, Rong Yang, Zi Yang Meng, Dongxia Shi, Oleg V. Yazyev, and Guangyu Zhang. Correlated states in twisted double bilayer graphene. *Nature Physics*, 16(5):520–525, May 2020.
- [74] Yuan Cao, Daniel Rodan-Legrain, Oriol Rubies-Bigorda, Jeong Min Park, Kenji Watanabe, Takashi Taniguchi, and Pablo Jarillo-Herrero. Tunable correlated states and spin-polarized phases in twisted bilayer–bilayer graphene. *Nature*, pages 1–6, May 2020.
- [75] Xiaomeng Liu, Zeyu Hao, Eslam Khalaf, Jong Yeon Lee, Kenji Watanabe, Takashi Taniguchi, Ashvin Vishwanath, and Philip Kim. Spin-polarized Correlated Insulator and Superconductor in Twisted Double Bilayer Graphene. *arXiv:1903.08130 [cond-mat]*, March 2019. arXiv: 1903.08130.
- [76] Guorui Chen, Lili Jiang, Shuang Wu, Bosai Lyu, Hongyuan Li, Bheema Lingam Chittari, Kenji Watanabe, Takashi Taniguchi, Zhiwen Shi, Jeil Jung, Yuanbo Zhang, and Feng Wang. Evidence of a gate-tunable Mott insulator in a trilayer graphene moiré superlattice. *Nature Physics*, 15(3):237, March 2019.
- [77] Guorui Chen, Aaron L. Sharpe, Patrick Gallagher, Ilan T. Rosen, Eli J. Fox, Lili Jiang, Bosai Lyu, Hongyuan Li, Kenji Watanabe, Takashi Taniguchi, Jeil Jung, Zhiwen Shi, David Goldhaber-Gordon, Yuanbo Zhang, and Feng Wang. Signatures of tunable superconductivity in a trilayer graphene moiré superlattice. *Nature*, 572(7768):215–219, August 2019.
- [78] Guorui Chen, Aaron L. Sharpe, Eli J. Fox, Ya-Hui Zhang, Shaoxin Wang, Lili Jiang, Bosai Lyu, Hongyuan Li, Kenji Watanabe, Takashi Taniguchi, Zhiwen Shi, T. Senthil, David Goldhaber-Gordon, Yuanbo Zhang, and Feng Wang. Tunable correlated Chern insulator and ferromagnetism in a moiré superlattice. *Nature*, 579(7797):56–61, March 2020.
- [79] G. William Burg, Biao Lian, Takashi Taniguchi, Kenji Watanabe, B. Andrei Bernevig, and Emanuel Tutuc. Evidence of emergent symmetry and valley chern number in twisted double-bilayer graphene, 2020.
- [80] Adrien Bouhon, Annica M. Black-Schaffer, and Robert-Jan Slager. Wilson loop approach to fragile topology of split elementary band representations and topological crystalline insulators with time-reversal symmetry. *Phys. Rev. B*, 100:195135, Nov 2019.

- [81] Kasra Hejazi, Chunxiao Liu, Hassan Shapourian, Xiao Chen, and Leon Balents. Multiple topological transitions in twisted bilayer graphene near the first magic angle. *Phys. Rev. B*, 99:035111, Jan 2019.
- [82] Kasra Hejazi, Chunxiao Liu, and Leon Balents. Landau levels in twisted bilayer graphene and semiclassical orbits. *Physical Review B*, 100(3), Jul 2019.
- [83] Xiao-Chuan Wu, Chao-Ming Jian, and Cenke Xu. Coupled-wire description of the correlated physics in twisted bilayer graphene. *Physical Review B*, 99(16), Apr 2019.
- [84] Alex Thomson, Shubhayu Chatterjee, Subir Sachdev, and Mathias S. Scheurer. Triangular antiferromagnetism on the honeycomb lattice of twisted bilayer graphene. *Physical Review B*, 98(7), Aug 2018.
- [85] Kangjun Seo, Valeri N. Kotov, and Bruno Uchoa. Ferromagnetic mott state in twisted graphene bilayers at the magic angle. *Phys. Rev. Lett.*, 122:246402, Jun 2019.
- [86] Kasra Hejazi, Xiao Chen, and Leon Balents. Hybrid wannier chern bands in magic angle twisted bilayer graphene and the quantized anomalous hall effect, 2020.
- [87] Maine Christos, Subir Sachdev, and Mathias Scheurer. Superconductivity, correlated insulators, and wess-zumino-witten terms in twisted bilayer graphene, 2020.
- [88] Cyprian Lewandowski, Debanjan Chowdhury, and Jonathan Ruhman. Pairing in magic-angle twisted bilayer graphene: role of phonon and plasmon umklapp, 2020.
- [89] Ming Xie and A. H. MacDonald. Nature of the correlated insulator states in twisted bilayer graphene. *Phys. Rev. Lett.*, 124:097601, Mar 2020.
- [90] Jianpeng Liu and Xi Dai. Theories for the correlated insulating states and quantum anomalous hall phenomena in twisted bilayer graphene, 2020.
- [91] Tommaso Cea and Francisco Guinea. Band structure and insulating states driven by coulomb interaction in twisted bilayer graphene. *Phys. Rev. B*, 102:045107, Jul 2020.
- [92] Yi Zhang, Kun Jiang, Ziqiang Wang, and Fuchun Zhang. Correlated insulating phases of twisted bilayer graphene at commensurate filling fractions: A hartree-fock study. *Phys. Rev. B*, 102:035136, Jul 2020.
- [93] Shang Liu, Eslam Khalaf, Jong Yeon Lee, and Ashvin Vishwanath. Nematic topological semimetal and insulator in magic angle bilayer graphene at charge neutrality, 2020.
- [94] Yuan Da Liao, Zi Yang Meng, and Xiao Yan Xu. Valence bond orders at charge neutrality in a possible two-orbital extended hubbard model for twisted bilayer graphene. *Phys. Rev. Lett.*, 123:157601, Oct 2019.
- [95] Yuan Da Liao, Jian Kang, Clara N. Breiø, Xiao Yan Xu, Han-Qing Wu, Brian M. Andersen, Rafael M. Fernandes, and Zi Yang Meng. Correlation-induced insulating topological phases at charge neutrality in twisted bilayer graphene, 2020.
- [96] Laura Classen, Carsten Honerkamp, and Michael M Scherer. Competing phases of interacting electrons on triangular lattices in moiré heterostructures. *Physical Review B*, 99(19):195120, 2019.
- [97] Dante M Kennes, Johannes Lischner, and Christoph Karrasch. Strong correlations and d+id superconductivity in twisted bilayer graphene. *Physical Review B*, 98(24):241407, 2018.
- [98] P Myles Eugenio and Ceren B Dağ. Dmrg study of strongly interacting z_2 flatbands: a toy model inspired by twisted bilayer graphene. *arXiv preprint arXiv:2004.10363*, 2020.
- [99] Yixuan Huang, Pavan Hosur, and Hridis K Pal. Deconstructing magic-angle physics in twisted bilayer graphene with a two-leg ladder model. *arXiv preprint arXiv:2004.10325*, 2020.
- [100] Tongyun Huang, Lufeng Zhang, and Tianxing Ma. Antiferromagnetically ordered mott insulator and d+id superconductivity in twisted bilayer graphene: A quantum monte carlo study. *Science Bulletin*, 64(5):310–314, 2019.
- [101] Huaiming Guo, Xingchuan Zhu, Shiping Feng, and Richard T Scalettar. Pairing symmetry of interacting fermions on a twisted bilayer graphene superlattice. *Physical Review B*, 97(23):235453, 2018.
- [102] Patrick J. Ledwith, Grigory Tarnopolsky, Eslam Khalaf, and Ashvin Vishwanath. Fractional chern insulator states in twisted bilayer graphene: An analytical approach. *Phys. Rev. Research*, 2:023237, May 2020.
- [103] Cécile Repellin, Zhihuan Dong, Ya-Hui Zhang, and T. Senthil. Ferromagnetism in narrow bands of moiré superlattices. *Phys. Rev. Lett.*, 124:187601, May 2020.
- [104] Ahmed Abouelkomsan, Zhao Liu, and Emil J. Bergholtz. Particle-hole duality, emergent fermi liquids, and fractional chern insulators in moiré flatbands. *Phys. Rev. Lett.*, 124:106803, Mar 2020.
- [105] Cécile Repellin and T. Senthil. Chern bands of twisted bilayer graphene: Fractional chern insulators and spin phase transition. *Phys. Rev. Research*, 2:023238, May 2020.
- [106] Oskar Vafek and Jian Kang. Towards the hidden symmetry in coulomb interacting twisted bilayer graphene: renormalization group approach, 2020.
- [107] Rafael M. Fernandes and Jörn W. F. Venderbos. Nematicity with a twist: Rotational symmetry breaking in a moiré superlattice. *Science Advances*, 6(32), 2020.
- [108] Jie Wang, Yunqin Zheng, Andrew J. Millis, and Jennifer Cano. Chiral approximation to twisted bilayer graphene: Exact intra-valley inversion symmetry, nodal structure and implications for higher magic angles, 2020.
- [109] B. Andrei Bernevig, Zhida Song, Nicolas Regnault, and Biao Lian. TBG I: Matrix elements, approximations, perturbation theory and a $k \cdot p$ 2-band model for twisted bilayer graphene. *arXiv e-prints*, page arXiv:2009.11301, September 2020.
- [110] B. Andrei Bernevig, Zhida Song, Nicolas Regnault, and Biao Lian. TBG III: Interacting hamiltonian and exact symmetries of twisted bilayer graphene. *arXiv e-prints*, page arXiv:2009.12376, September 2020.
- [111] Biao Lian, Zhi-Da Song, Nicolas Regnault, Dmitri K. Efetov, Ali Yazdani, and B. Andrei Bernevig. Tbg iv: Exact insulator ground states and phase diagram of twisted bilayer graphene. *arXiv e-prints*, page arXiv:2009.13530, September 2020.
- [112] B. Andrei Bernevig, Biao Lian, Aditya Cowsik, Fang Xie, Nicolas Regnault, and Zhi-Da Song. TBG V: Exact analytic many-body excitations in twisted bilayer graphene coulomb hamiltonians: Charge gap, goldstone modes and absence of cooper pairing. *arXiv e-prints*, page arXiv:2009.14200, September 2020.
- [113] Fang Xie, Aditya Cowsik, Zhida Song, Biao Lian, B. Andrei Bernevig, and Nicolas Regnault. TBG VI: An ex-

- act diagonalization study of twisted bilayer graphene at non-zero integer fillings. *arXiv e-prints*, page arXiv:2010.00588, September 2020.
- [114] Hoi Chun Po, Haruki Watanabe, and Ashvin Vishwanath. Fragile Topology and Wannier Obstructions. *Physical Review Letters*, 121(12):126402, September 2018.
- [115] Jennifer Cano, Barry Bradlyn, Zhijun Wang, L. Elcoro, M. G. Vergniory, C. Felser, M. I. Aroyo, and B. Andrei Bernevig. Topology of disconnected elementary band representations. *Phys. Rev. Lett.*, 120:266401, Jun 2018.
- [116] Dominic V. Else, Hoi Chun Po, and Haruki Watanabe. Fragile topological phases in interacting systems. *Phys. Rev. B*, 99:125122, Mar 2019.
- [117] Juan L. Mañes. Fragile phonon topology on the honeycomb lattice with time-reversal symmetry. *Phys. Rev. B*, 102:024307, Jul 2020.
- [118] A. Alexandradinata, J. Höller, Chong Wang, Hengbin Cheng, and Ling Lu. Crystallographic splitting theorem for band representations and fragile topological photonic crystals. *Phys. Rev. B*, 102:115117, Sep 2020.
- [119] Kazuyuki Uchida, Shinnosuke Furuya, Jun-Ichi Iwata, and Atsushi Oshiyama. Atomic corrugation and electron localization due to moiré patterns in twisted bilayer graphenes. *Phys. Rev. B*, 90:155451, Oct 2014.
- [120] M M van Wijk, A Schuring, M I Katsnelson, and A Fasolino. Relaxation of moiré patterns for slightly misaligned identical lattices: graphene on graphite. *2D Materials*, 2(3):034010, Jul 2015.
- [121] Shuyang Dai, Yang Xiang, and David J Srolovitz. Twisted bilayer graphene: Moiré with a twist. *Nano letters*, 16(9):5923–5927, 2016.
- [122] Sandeep K Jain, Vladimir Juričić, and Gerard T Barkema. Structure of twisted and buckled bilayer graphene. *2D Materials*, 4(1):015018, Nov 2016.
- [123] Samuel V Gallego, Emre S Tasci, G Flor, J Manuel Perez-Mato, and Mois I Aroyo. Magnetic symmetry in the Bilbao crystallographic server: a computer program to provide systematic absences of magnetic neutron diffraction. *Journal of Applied Crystallography*, 45(6):1236–1247, 2012.
- [124] A Alexandradinata, Zhijun Wang, and B Andrei Bernevig. Topological insulators from group cohomology. *Physical Review X*, 6(2):021008, 2016.
- [125] Zhijun Wang, Aris Alexandradinata, Robert J Cava, and B Andrei Bernevig. Hourglass fermions. *Nature*, 532(7598):189–194, 2016.
- [126] Rui Yu, Xiao Liang Qi, Andrei Bernevig, Zhong Fang, and Xi Dai. Equivalent expression of \mathbb{Z}_2 topological invariant for band insulators using the non-Abelian Berry connection. *Phys. Rev. B*, 84(7):075119, August 2011.
- [127] A. Alexandradinata, Xi Dai, and B. Andrei Bernevig. Wilson-loop characterization of inversion-symmetric topological insulators. *Phys. Rev. B*, 89:155114, Apr 2014.
- [128] Liang Fu and C. L. Kane. Time reversal polarization and a Z_2 adiabatic spin pump. *Phys. Rev. B*, 74:195312, Nov 2006.
- [129] Takahiro Fukui and Yasuhiro Hatsugai. Quantum spin hall effect in three dimensional materials: Lattice computation of \mathbb{Z}_2 topological invariants and its application to bi and sb. *Journal of the Physical Society of Japan*, 76(5):053702–053702, 2007.
- [130] B. Andrei Bernevig and Taylor L. Hughes. *Topological Insulators and Topological Superconductors*. Princeton University Press, 2013.
- [131] Junyeong Ahn, Dongwook Kim, Youngkuk Kim, and Bohm-Jung Yang. Band Topology and Linking Structure of Nodal Line Semimetals with \mathbb{Z}_2 Monopole Charges. *Physical Review Letters*, 121(10):106403, September 2018.
- [132] F. Nur Ünal, Adrien Bouhon, and Robert-Jan Slager. Topological euler class as a dynamical observable in optical lattices. *Phys. Rev. Lett.*, 125:053601, Jul 2020.
- [133] QuanSheng Wu, Alexey A Soluyanov, and Tomáš Bzdušek. Non-abelian band topology in noninteracting metals. *Science*, 365(6459):1273–1277, 2019.
- [134] Christophe Mora, Nicolas Regnault, and B. Andrei Bernevig. Flatbands and perfect metal in trilayer moiré graphene. *Phys. Rev. Lett.*, 123:026402, Jul 2019.
- [135] Chen Fang, Matthew J. Gilbert, and B. Andrei Bernevig. Bulk topological invariants in noninteracting point group symmetric insulators. *Phys. Rev. B*, 86(11):115112, September 2012.
- [136] Taylor L. Hughes, Emil Prodan, and B. Andrei Bernevig. Inversion-symmetric topological insulators. *Phys. Rev. B*, 83:245132, Jun 2011.
- [137] Ari M. Turner, Yi Zhang, Roger S. K. Mong, and Ashvin Vishwanath. Quantized response and topology of magnetic insulators with inversion symmetry. *Phys. Rev. B*, 85:165120, Apr 2012.

A. Hamiltonian of twisted bilayer graphene in momentum space

1. The Hamiltonian

Here we briefly introduce the momentum space Hamiltonian $H(\mathbf{k})$ corresponding to Eq. (1). Readers may refer to the supplementary materials of Ref. [58] for more details. The basis of $H(\mathbf{k})$ is $|\phi_{\mathbf{Q},\alpha}(\mathbf{k})\rangle$, where \mathbf{k} is a momentum in the moiré BZ, \mathbf{Q} is a point in the lattice shown in Fig. 6, and $\alpha = 1, 2$ is the sublattice index of graphene. There are two types of \mathbf{Q} lattices: the blue lattice \mathcal{Q}_T and the red lattice \mathcal{Q}_B . For $\mathbf{Q} \in \mathcal{Q}_T$, the basis $|\phi_{\mathbf{Q},\alpha}(\mathbf{k})\rangle$ is a plane-wave state from the top layer

$$|\phi_{\mathbf{Q},\alpha}(\mathbf{k})\rangle = \frac{1}{\sqrt{N}} \sum_{\mathbf{R}} e^{i(\mathbf{R}+\mathbf{t}_\alpha) \cdot (\mathbf{k} - \mathbf{Q})} |\mathbf{R} + \mathbf{t}_\alpha\rangle, \quad (\text{A1})$$

where N is the number of lattices in the top layer graphene, \mathbf{R} indexes all the lattices of the top layer graphene, \mathbf{t}_α is the sublattice vector of the top layer graphene, $|\mathbf{R} + \mathbf{t}_\alpha\rangle$ is the atomic orbital at $\mathbf{R} + \mathbf{t}_\alpha$. For $\mathbf{Q} \in \mathcal{Q}_B$, the basis $|\phi_{\mathbf{Q},\alpha}(\mathbf{k})\rangle$ is a plane-wave state from the bottom layer

$$|\phi_{\mathbf{Q},\alpha}(\mathbf{k})\rangle = \frac{1}{\sqrt{N}} \sum_{\mathbf{R}^0} e^{i(\mathbf{R}^0+\mathbf{t}_\alpha^0) \cdot (\mathbf{k} - \mathbf{Q})} |\mathbf{R}^0 + \mathbf{t}_\alpha^0\rangle, \quad (\text{A2})$$

where N is the number of lattices in the bottom layer graphene (same as the one in top layer), \mathbf{R}^0 indexes all the lattices of the bottom layer graphene, \mathbf{t}_α^0 is the sublattice vector of the bottom layer graphene, $|\mathbf{R}^0 + \mathbf{t}_\alpha^0\rangle$ is the atomic orbital at $\mathbf{R}^0 + \mathbf{t}_\alpha^0$. The Hamiltonian (Eq. (1)) on the basis $|\phi_{\mathbf{Q},\alpha}(\mathbf{k})\rangle$ is given by

$$H_{\mathbf{Q},\mathbf{Q}'}(\mathbf{k}) = v_F \delta_{\mathbf{Q},\mathbf{Q}'} (\mathbf{k} - \mathbf{Q}) \cdot \boldsymbol{\sigma} - \frac{\theta}{2} \zeta_{\mathbf{Q}} \delta_{\mathbf{Q},\mathbf{Q}'} (\mathbf{k} - \mathbf{Q}) \times \boldsymbol{\sigma} + \sum_{j=1}^3 (\delta_{\mathbf{Q}'}^{\mathbf{Q},\mathbf{q}_j} + \delta_{\mathbf{Q}}^{\mathbf{Q}',\mathbf{q}_j}) T_j, \quad (\text{A3})$$

where $\boldsymbol{\sigma} = (\sigma_x, \sigma_y)$ and T_j ($j = 1, 2, 3$) are two-by-two matrices in the sublattice space, $\zeta_{\mathbf{Q}} = 1$ for $\mathbf{Q} \in \mathcal{Q}_T$ and $\zeta_{\mathbf{Q}} = -1$ for $\mathbf{Q} \in \mathcal{Q}_B$.

2. The periodicity of Bloch states

An eigenstate of Eq. (1) at a given momentum \mathbf{k} can be written as linear combination of the Bloch basis as $|\psi_n(\mathbf{k})\rangle = \sum_{\mathbf{Q},\alpha} |\phi_{\mathbf{Q},\alpha}(\mathbf{k})\rangle u_{\mathbf{Q},\alpha,n}(\mathbf{k})$. Here n is the band index. It should be noticed that the basis states in Eqs. (A1) and (A2) are *not* periodic in the moiré BZ since $|\phi_{\mathbf{Q},\alpha}(\mathbf{k} + \mathbf{G})\rangle = |\psi_{\mathbf{Q} - \mathbf{G},\alpha}(\mathbf{k})\rangle$ by definition. In order for the Bloch state $|\psi_n(\mathbf{k})\rangle$ to be periodic in the moiré BZ, *i.e.*, $|\psi_n(\mathbf{k} + \mathbf{G})\rangle = |\psi_n(\mathbf{k})\rangle$, $u_{\mathbf{Q},\alpha,n}(\mathbf{k})$ should satisfy $u_{\mathbf{Q},\alpha,n}(\mathbf{k} + \mathbf{G}) = u_{\mathbf{Q} - \mathbf{G},\alpha,n}(\mathbf{k})$. We introduce the embedding matrix

$$V_{\mathbf{Q},\mathbf{Q}'}^{\mathbf{G}} = \delta_{\mathbf{Q} - \mathbf{G},\mathbf{Q}'} \quad (\text{A4})$$

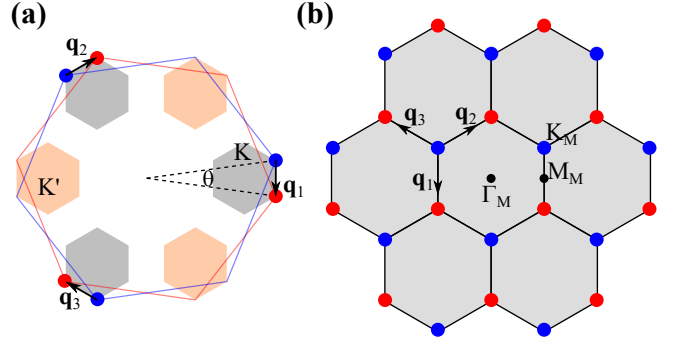


FIG. 6. The \mathbf{Q} -lattice for the momentum space Hamiltonian of twisted bilayer graphene. (a) The blue and red hexagons represent the Brillouin zones of the top layer and the bottom layer, respectively. The blue and red dots represent the positions of Dirac points of the two layers in the graphene valley K , respectively. (b) The \mathbf{Q} lattice formed by adding $\mathbf{q}_{1,2,3}$ iteratively. At each blue dot a plane-wave state from the top layer is assigned, and at each red dot a plane-wave state from the bottom layer is assigned.

such that we can write the periodicity of Bloch states as

$$|u_n(\mathbf{k} + \mathbf{G})\rangle = V^{\mathbf{G}} |u_n(\mathbf{k})\rangle, \quad (\text{A5})$$

where $|u_n(\mathbf{k})\rangle = (u_{\mathbf{Q}_1,1,n}(\mathbf{k}), u_{\mathbf{Q}_1,2,n}(\mathbf{k}), u_{\mathbf{Q}_2,1,n}(\mathbf{k}) \dots)^T$. While exact Bloch periodicity requires that the cutoff in the lattice \mathbf{Q} be large, we have showed - around the first magic angle - [109] that we can obtain machine precision accuracy in the first moiré BZ by taking a small cutoff in \mathbf{Q}

3. Symmetry operators in the momentum space

The crystalline symmetry group of the single valley Hamiltonian is the magnetic space group $P6^0_2O_2$ (#177.151 in the BNS setting [123]). The generators of this group are: The C_{3z} symmetry

$$H(C_{3z}\mathbf{k}) = D(C_{3z}) H(C_{3z}\mathbf{k}) D^\dagger(C_{3z}) \quad (\text{A6})$$

where $D_{\mathbf{Q}',\mathbf{Q}}(C_{3z}) = e^{i\frac{2\pi}{3}\sigma_z} \delta_{\mathbf{Q}',C_{3z}\mathbf{Q}}$. The C_{2x} symmetry

$$H(C_{2x}\mathbf{k}) = D(C_{2x}) H(C_{2x}\mathbf{k}) D^\dagger(C_{2x}) \quad (\text{A7})$$

where $D_{\mathbf{Q}',\mathbf{Q}}(C_{2x}) = \sigma_x \delta_{\mathbf{Q}',C_{2x}\mathbf{Q}}$, and $C_{2x}\mathbf{q}_1 = -\mathbf{q}_1$. The $C_{2z}T$ symmetry

$$H(\mathbf{k}) = D(C_{2z}T) H_{\mathbf{Q},\mathbf{Q}'}(\mathbf{k}) D^\dagger(C_{2z}T) \quad (\text{A8})$$

where $D_{\mathbf{Q}',\mathbf{Q}}(C_{2z}T) = \sigma_x \delta_{\mathbf{Q}',\mathbf{Q}}$. It should be noticed that all rotations of momenta here are with respect to the Γ_M point of the moiré BZ.

When the second term in Eq. (A3) is negligible, $H(\mathbf{k})$ has an emergent unitary particle-hole symmetry

$$H(-\mathbf{k}) = -D(P) H(\mathbf{k}) D^\dagger(P) \quad (\text{A9})$$

where $D_{\mathbf{Q},\mathbf{Q}'}(P) = \delta_{\mathbf{Q},\mathbf{Q}'}$, $\mathbf{Q}\zeta_{\mathbf{Q}}$, and $\zeta_{\mathbf{Q}} = 1$ for $\mathbf{Q} \in \mathcal{Q}_T$ and $\zeta_{\mathbf{Q}} = -1$ for $\mathbf{Q} \in \mathcal{Q}_B$. The anti-unitary particle-hole symmetry $\mathcal{P} = PC_{2z}T$ in momentum space is

$$H(-\mathbf{k}) = -D(\mathcal{P})H(-\mathbf{k})D^T(\mathcal{P}), \quad (\text{A10})$$

where $D_{\mathbf{Q},\mathbf{Q}'}(\mathcal{P}) = \sigma_x \delta_{\mathbf{Q},\mathbf{Q}'}$, $\mathbf{Q}\zeta_{\mathbf{Q}}$. When $w_0 = 0$, $H(\mathbf{k})$ has an emergent chiral symmetry

$$H(\mathbf{k}) = -D^y(C)H(\mathbf{k})D(C), \quad (\text{A11})$$

where $D_{\mathbf{Q},\mathbf{Q}'}(C) = \sigma_z \delta_{\mathbf{Q},\mathbf{Q}'}$. When $w_1 = 0$, $H(\mathbf{k})$ has another emergent chiral symmetry (the second chiral symmetry)

$$H(\mathbf{k}) = -D^y(C^0)H(\mathbf{k})D(C^0), \quad (\text{A12})$$

where $D_{\mathbf{Q},\mathbf{Q}'}(C^0) = \sigma_z \delta_{\mathbf{Q},\mathbf{Q}'}$, $\zeta_{\mathbf{Q}}$.

The embedding matrix transform under the unitary operators ($g = C_{3z}, C_{2x}, P, C, C^0$) as

$$D(g)V^G D^y(g) = V^g G. \quad (\text{A13})$$

For the unitary operator $C_{2z}T$, we have

$$D(C_{2z}T)V^G D^T(C_{2z}T) = V^G. \quad (\text{A14})$$

One can verify that the two identities by explicitly acting the symmetry operators on the embedding matrix.

4. The sewing matrices of symmetry operators

For the unitary crystalline symmetries, *e.g.*, $g = C_{3z}, C_{2x}, P, C, C^0$, we define the sewing matrices as

$$B_{n'n}^{(g)}(\mathbf{k}) = \langle u_{n'}(g\mathbf{k}) | D(g) | u_n(\mathbf{k}) \rangle. \quad (\text{A15})$$

For the anti-unitary symmetries, *e.g.*, $g = C_{2z}T, \mathcal{P}$, we define the sewing matrices as

$$B_{n'n}^{(g)}(\mathbf{k}) = \langle u_{n'}(g\mathbf{k}) | D(g) | u_n(\mathbf{k}) \rangle. \quad (\text{A16})$$

Using the identities Eqs. (A13) and (A14), we obtain that the sewing matrices are periodic in momentum space, *i.e.*, $B^{(g)}(\mathbf{k} + \mathbf{G}) = B^{(g)}(\mathbf{k})$ for arbitrary reciprocal lattice \mathbf{G} . The explicit expression for the sewing matrices depend on different basis, and will be give in Ref. [110] for the cases needed for our interacting problem.

B. The gauge of Chern band basis

In Section V we have explained that the choice of Chern band basis due to the $C_{2z}T$ gauge fixing (Eq. (26)) has two ambiguities: (i) the choice of the two branches of $\frac{\theta_n(\mathbf{k})}{2}$, *i.e.*, $\frac{\theta_n(\mathbf{k})}{2}$ and $\frac{\theta_n(\mathbf{k})}{2} + \pi$, and (ii) the choice of $|u_1(\mathbf{k})\rangle$ and $|u_{-1}(\mathbf{k})\rangle$ at Dirac points where the two bands are degenerate. Both ambiguities lead to an ambiguity when choosing $|v(\mathbf{k})\rangle$. If we replace $\frac{\theta_1(\mathbf{k})}{2}$ by $\frac{\theta_1(\mathbf{k})}{2} + \pi$

in Eq. (26), then the two Chern band states in the new gauge $|v^0(\mathbf{k})\rangle$ are related to the Chern band states in the previous gauge as

$$\begin{aligned} |v^0(\mathbf{k})\rangle &= \frac{1}{\sqrt{2}}(-e^{i\frac{\theta_1(\mathbf{k})}{2}}|u_1(\mathbf{k})\rangle \pm ie^{i\frac{\theta_{-1}(\mathbf{k})}{2}}|u_{-1}(\mathbf{k})\rangle) \\ &= -|v(\mathbf{k})\rangle. \end{aligned} \quad (\text{B1})$$

Therefore, changing the branch of $\frac{\theta_1(\mathbf{k})}{2}$ at \mathbf{k} will interchange the two states $|v(\mathbf{k})\rangle$ at \mathbf{k} . One can show that changing the branch of $\frac{\theta_{-1}(\mathbf{k})}{2}$ will also interchange the two states $|v(\mathbf{k})\rangle$ for the same reason. We then consider to interchange $|u_{-1}(\mathbf{k})\rangle$ at a Dirac point \mathbf{k}_D . The Chern band states $|v^{00}(\mathbf{k}_D)\rangle$ defined with the interchanged $|u_{-1}(\mathbf{k}_D)\rangle$ become

$$\begin{aligned} |v^{00}(\mathbf{k}_D)\rangle &= \frac{1}{\sqrt{2}}(e^{i\frac{\theta_{-1}(\mathbf{k}_D)}{2}}|u_{-1}(\mathbf{k}_D)\rangle \pm ie^{i\frac{\theta_1(\mathbf{k}_D)}{2}}|u_1(\mathbf{k}_D)\rangle) \\ &= \pm |v(\mathbf{k})\rangle. \end{aligned} \quad (\text{B2})$$

Thus interchanging $|u_{-1}(\mathbf{k})\rangle$ at Dirac points will interchange $|v(\mathbf{k})\rangle$ at the Dirac points.

Due to the ambiguities discussed above, at each \mathbf{k} point we only have two choices for $|v(\mathbf{k})\rangle$ (up to phase factors). Starting with $|v(\mathbf{k}_0)\rangle$ at a given momentum \mathbf{k}_0 , the condition Eq. (27) will uniquely determine the two branches of $|v(\mathbf{k})\rangle$ over the whole BZ. To be specific, we consider the choice of $|v(\mathbf{k}_0 + \mathbf{q})\rangle$ for \mathbf{q} being a small momentum. Suppose $|v^0(\mathbf{k}_0 + \mathbf{q})\rangle$ is returned by Eq. (26) without considering Eq. (27). Then if they satisfy $|\langle v_m(\mathbf{k}_0) | v_{m'}^0(\mathbf{k}_0 + \mathbf{q}) \rangle| \approx \delta_{mm'}$, we choose $|v(\mathbf{k}_0 + \mathbf{q})\rangle = |v^0(\mathbf{k}_0 + \mathbf{q})\rangle$; otherwise, *i.e.*, $|\langle v_m(\mathbf{k}_0) | v_{m'}^0(\mathbf{k}_0 + \mathbf{q}) \rangle| \approx 1 - \delta_{mm'}$, we choose $|v(\mathbf{k}_0 + \mathbf{q})\rangle = |v^0(\mathbf{k}_0 + \mathbf{q})\rangle$. Repeating this procedure over the whole BZ iteratively will uniquely determined the two branches of $|v(\mathbf{k})\rangle$.

We now explain that the obtained two branches by the method introduced above must be Chern bands. We first consider \mathbf{k} not at the Dirac points. Due to the discussion in Section V, if a smooth branch of $\frac{\theta_n(\mathbf{k})}{2}$ is chosen, the states $|v(\mathbf{k})\rangle$ will have smooth Berry's curvatures $\pm f(\mathbf{k})$. On the other hand, if the branch of $\frac{\theta_n(\mathbf{k})}{2}$ changes at \mathbf{k}_* , then there is $\lim_{\mathbf{q} \rightarrow 0} |\langle v_+(\mathbf{k}_*) | v_+(\mathbf{k}_* + \mathbf{q}) \rangle| = |\langle v_+(\mathbf{k}_*) | v(\mathbf{k}_*) \rangle| = 0$ and hence the Berry's curvatures of $|v(\mathbf{k})\rangle$ will be discontinuous at \mathbf{k}_* . Therefore, choosing a smooth branch of $\frac{\theta_n(\mathbf{k})}{2}$ is equivalent to choosing $|v(\mathbf{k})\rangle$ such that they have continuous Berry's curvatures. Thus Eq. (27), which guarantees continuous Berry's curvatures, also enforces that $|v(\mathbf{k})\rangle$ must have the Berry's curvatures $\pm f(\mathbf{k})$. We then consider the Dirac points. Since there is a finite number of Dirac points in the BZ, the integral of Berry's curvature in the (infinite small) neighborhoods of the Dirac points approaches zero as long as Eq. (27) holds such that the Berry's curvature is non-divergent. Therefore, the integral of Berry's curvatures of $|v(\mathbf{k})\rangle$ subject to the condition Eq. (27) are $\pm \frac{1}{2\pi} \int d^2\mathbf{k} f(\mathbf{k}) = \pm e_2$.

Now we explicitly show why the Berry's curvatures of Eq. (26) are not divergent at the Dirac points if Eq. (27)

holds. We consider a linearized k-p model around a single Dirac point $H = k_x \sigma_x + k_y \sigma_y$, where the $C_{2z}T$ operator is $\sigma_x \bar{K}$. Since Berry's curvature is gauge-invariant, we take the particular gauge $\theta_1(\mathbf{k}) = \theta_{-1}(\mathbf{k}) = 0$ in the calculation. The Bloch states in this gauge are

$$|u_1(\mathbf{k})\rangle = \frac{1}{\sqrt{2}} \begin{pmatrix} e^{-i\frac{\phi(\mathbf{k})}{2}} \\ e^{i\frac{\phi(\mathbf{k})}{2}} \end{pmatrix}, \quad |u_{-1}(\mathbf{k})\rangle = \frac{1}{\sqrt{2}} \begin{pmatrix} -ie^{-i\frac{\phi(\mathbf{k})}{2}} \\ ie^{i\frac{\phi(\mathbf{k})}{2}} \end{pmatrix}, \quad (\text{B3})$$

where $\phi(\mathbf{k}) = \arccos \frac{k_x}{\sqrt{k_x^2 + k_y^2}}$. Then the recombined Chern basis are $|v_+(\mathbf{k})\rangle = (e^{i\frac{\phi(\mathbf{k})}{2}}, 0)^T$, $|v_-(\mathbf{k})\rangle = (0, e^{i\frac{\phi(\mathbf{k})}{2}})^T$. They satisfy Eq. (27) and have vanishing Berry's curvatures in the neighbourhood of the Dirac point.